Lawrence Berkeley National Laboratory

Recent Work

Title

Structure and Mechanical Adaptability of a Modern Elasmoid Fish Scale from the Common Carp

Permalink

https://escholarship.org/uc/item/045972gs

Journal

Matter, 3(3)

ISSN

2590-2393

Authors

Quan, H
Yang, W
Lapeyriere, M
et al.

Publication Date

2020-09-02

DOI

10.1016/j.matt.2020.05.011

Peer reviewed

eScholarship.org Powered by the California Digital Library
University of California

H. Quan, *et al*., Structure and mechanical adaptability of a modern elasmoid fish scale from the common carp, *Matter*, vol. 3 (3), Sept. 2020, pp. 842-863; doi.org/10.1016/j.matt.2020.05.011.

Structure and mechanical adaptability of a modern elasmoid fish scale from the common carp

Haocheng Quan[1‡], Wen Yang[1,2‡*], Marine Lapeyriere[1], Eric Schaible[3], Robert O. Ritchie[2,4,5*] & Marc A. Meyers[1]

[1] Materials Science and Engineering Program, University of California, San Diego, California 92093, USA

[2] Materials Sciences Division, Lawrence Berkeley National Laboratory, Berkeley, California 94720, USA

[3] Advanced Light Source, Lawrence Berkeley National Laboratory, Berkeley, California 94720, USA

[4] Department of Materials Science and Engineering, University of California, Berkeley, California 94720, USA

[5] Lead Contact

[‡] These authors contributed equally.

*Corresponding authors. e-mail addresses: wey005@eng.ucsd.edu & roritchie@lbl.gov

SUMMARY

The carp (*Cyprinus carpio*) has typical elasmoid scales commonly found on teleosts. They provide protection while retaining flexibility and maneuverability of the fish. The exterior surface of the scale consists of an ultra-thin discontinuous mineral layer on top of mineralized woven collagen fibrils. The underlying foundation is composed of two collagenous components. The major one consists of a single-twisted "Bouligand" structure, with a twisting angle of 36°. A secondary "sheet-like" structure, formed by thinner collagen fibrils oriented along the thickness direction, acts to increase the integrity of the scale. Here we identify the deformation and failure mechanisms of the carp scale, revealing slight tensile anisotropy. Using *in situ* small-angle x-ray scattering during tensile testing, the toughening mechanisms of the scale, including the adaptive structural reorientation of lamellae, as well as fibrillar sliding and elastic deformation, are quantified and compared with those of other fish scales.

Keywords: fish scales; teleost; dermal armor; Bouligand structure; carp

INTRODUCTION

The integument of vertebrates is a continuous and heterogeneous layer covering the body surface. It consists of two distinct strata: the epidermis and the dermis.[1] The epidermis is mainly composed of keratin with a stratified structure, playing a crucial role as a permeability barrier and mechanical protection.[1,2] Within it, many specialized cells are also able to develop non-skeletal epidermal scales, such as the ones in pangolin, and appendages like feathers, hooves, hairs, claws, beaks and nails, serving as multifunctional structural materials (armor, weapons, transportation tools, and thermal protection) to carry out assorted functions for organisms surviving in diverse environments.[2,3] The deep counterpart to the epidermis is the dermis, which is collagen-based.[1] The ability to mineralize the dermis layer is a major innovation for many lower vertebrates and has enabled them to develop an efficient protective shelter, also called "dermal armor", to prevent tissue damage caused by predatory attack.[4,5] The fish scale is the most common one, providing effective protection for the overwhelming majority of fish species living from tropical to polar regions.

Based on the histological and histochemical characteristics, the scales of the current existing fish are mainly grouped into placoid, ganoid, elasmoid, dermal plates and scutes.[1] The placoid scale is characteristic of cartilaginous fish, such as sharks and rays. The ganoid scale, another primitive category, is also called rhombic scale because of its diamond shape. There are mainly two types of ganoid scales existing currently: the quad-layered one, which is unique to *polypteriformes* (bichirs and reedfish) and the double-layered one, which is commonly found on *lepisosteiformes* (gars).[6,7] The scutes and dermal plates are also rigid fish scales, being modified from ganoid

scales.[1] The scutes are composed of a thick bony base capped by a layer of non-collagenous hyper-mineralized tissue called “hyaloine”, while the dermal plates are composed exclusively of bone. The most common example of a fish possessing scutes is the armored catfish (*callichthyids, loricariids and doradids*); dermal plates are also usually found in sturgeons, paddlefish, sticklebacks, boxfish, pufferfish, and seahorses.[1] Due to their rigidity, scutes and dermal plates are only able to provide protection for limited fish species, compared with the most evolved type, the elasmoid scale.

The elasmoid scale is, without any question, the most prominent dermal armor among living vertebrates, including most of current fish species and some gymnophionan amphibians.[1,8] The scales are thin collagenous plates embedded in the dermal pocket with roughly two-thirds of posterior surface overlapped by neighboring scales. Although considerably diverse in morphology and ornamentation (including both ctenoid and cycloid shapes), all elasmoid scales have a similar fundamental structure, which consists of three layers.[1,9,10] In the developmental sequence,[10] the first one to be formed is the external layer, which is an ornamented thin layer comprised of minerals (mainly hydroxyapatites) and well-mineralized, randomly-oriented collagen fibrils (woven fibrils). The second one to be formed is the tissue beneath the external layer, which is a thick basal plate composed of larger collagen fibrils forming a laminated plywood structure called “elasmodine”, where the name of elasmoid scales originates from. This plywood tissue (elasmodine) is slightly mineralized or completely unmineralized, resulting in great deformability for the scales. The last component to be formed is an extremely thin layer between the surface and the laminated (elasmodine) layers which is composed of pure mineral and is referred to as the “limiting layer”.[22,26,31] Based on previous studies on the structure and

mechanical behavior of elasmoid scales in various fish species, including arapaima,[11-18] red sea bream,[19] bass[20,21] and tarpon,[22] the protection mechanisms of elasmoid scales have been characterized: the well-mineralized outer layer, including the external layer and limiting layer, provides hardness against the bite from a predator's attack, and the soft collagenous laminated base enables great deformability to dissipate the stored elastic energy through assorted mechanisms, such as lamellar rotation and separation, collagen fibril stretching/compression, fibrillar delamination and bridging. The synergy of these mechanisms leads to outstanding scale toughness. By using primarily biopolymers and minerals in an intricate and ingenious hierarchical architecture, the elasmoid scales combine sufficient strength with excellent damage tolerance, properties that are often exclusive to synthetic materials, making these scales high-performance structural materials.[23,24]

Here, we cast our interest on the elasmoid scales of the common carp (*Cyprinus carpio*). As a typical dermal armor, the scales protect carps and enable them to survive in various environments globally. Although the structure and some mechanical properties of carp scale have already been studied,[25-31] the ultrafine structure of its collagenous lamellae has not been thoroughly investigated and the deformation mechanisms have not been quantified. In this work, we unravel the detailed structure of the carp scale, in particular using transmission electron microscopy (TEM) to characterize the ultrafine structure of the collagen fibrils in the lamellar inner core. We find that there are two collagenous frames comprising the plywood base of carp scale. The first one is composed of the collagenous lamellae made of isolated collagen fibrils; the arrangement of their orientations follows a helical pattern. The second one is a set of several layers composed of thinner collagen fibrils and forming a "sheet-like" structure oriented from the

basal part towards the external surface layer. In addition to conventional tensile testing, we also employed *in situ* synchrotron small-angle x-ray scattering (SAXS) measurements during the tensile deformation to quantify the lamellar rotation and collagen fibril stretching/compression. The deformation mechanisms of this well-evolved elasmoid scale are identified and compared with the primitive elasmoid scales from the living fossil coelacanth. This evaluation of the principal features is expected to generate critical thinking on the design of new synthetic structural materials.

RESULTS AND DISCUSSION

Hierarchical Structure of the Scales of the Common Carp

The common carp (*Cyprinus carpio*) is a widespread freshwater teleost from the family *Cyprinidae* which originated from eutrophic waters in lakes and large rivers in Europe and Asia. Their body is fully covered by imbricated/overlapped elasmoid scales anchored in the dermis pocket, as shown in Figure 1a. Each scale has an oval-like shape and 2/3 of its surface, the white part shown in Figure 1b, is covered by neighboring scales, which distributes stresses from a bite across a large volume of material and provides penetration resistance at a reduced weight.[32] Figures 1c-i manifest the surface characteristics of the scale's exterior surface (named the limiting or osseous layer due to its high degree of mineralization) and the external layer (~ 40 to 50 μm thick). The well mineralized limiting layer covers the external surface except at the periphery which is different from the other type of elasmoid scale, such as coelacanth fish scale, which contains pulp cavities in the external layer on the exposed region.[33,34] The carp scale does not have these pulp cavities on the exposed (posterior) region. Instead, the posterior region (dark region shown in Fig. 1b) has numerous mineral denticles scattered on it (Fig. 1c). A close-up

view of an isolated denticle, shown in Figure 1d, indicates that it is embedded in the dermis which is composed of randomly oriented collagen fibrils (Fig. 1e). The overlapped surface, presented in Figures 1f,g at different magnifications, shows two ornamentation characteristics: the *circuli*, as indicated by the dotted lines, and *radii*, indicated by the arrows. The *circuli* are concentric ridges or elevations on the superficial layer (dotted lines in Figs. 1f,g); in some primitive fish species like coelacanth or bowfin fish, they are in a radial position.[8,33] The *radii*, as indicated by the arrows in Figures 1f,g, are the linear grooves starting from the focal region of the scale and intersecting *circuli*. These features aid the anchoring of the scales in the dermis pocket and improve their stability.[35,36] A close-up view of the *circuli* (Fig. 1g) shows the regularity of their arrangement, with an approximately equal spacing. Mineralized thin woven fibrils (~30 - 50 nm in diameter) are observed in the space between *circuli* ridges (Fig. 1h), forming a randomly oriented loose network; this indicates that the limiting layer is extremely thin and discontinuous, leading to the partially exposed external fibrous layer. We compared the mineral contents of three types of elasmoid scales (carp, coelacanth and arapaima) by performing thermogravimetric analysis (TGA); the results, provided in Figure S1 in the Supplementary Information, show that the carp scale has the lowest mineral content. The cross-sectional view (Figs. 1i,j) also confirms our observations on the thickness of limiting and external layers; it also reveals the multilayered structure for carp scales, *i.e.,* beneath the limiting layer and the external layer, which has been identified on the top surface, is the elasmodine (Bouligand) layer, which is the major component of the scale. The detailed structure of this layer will be unraveled later. Figure 1i also reveals that the elasmodine, which is the laminated inner structure of the scale, is composed of two groups of collagen layers with different mineralization.[12] The outer (upper)

portions of the collagenous lamellae are more mineralized than the lower portion, as further shown in Figure S2.

Scanning electron microscopy (SEM) images of the oblique surface of freeze-fractured scales, provided in Figures 2a-c, disclose the structural characteristics of the inner layer. The internal layer of the scale represents the stacking of collagenous lamellae to form a plywood-like arrangement that occupies a major volume fraction of the scale. The collagen fibrils in each lamella are assembled in parallel, but the orientations of successive lamellae are offset by a specific angle. For a better understanding of the uniqueness of the carp scale's structure, SEM images of the coelacanth are presented in Figures 2d-f,[33] for comparison. There are three distinct features:

1. *Arrangements of lamellae orientation:* As the arrows indicate in Figure 2a, the orientations of successive lamellae in the carp scale form a helicoidal pattern from interior to exterior, named the "Bouligand" structure. The rotation angle (determined by the SAXS experiments described below) is ~36°. A similar helical pattern is also observed in the basal plate of arapaima[14] and tarpon scales.[22] In contrast, the lamellae orientations in coelacanth scale form a double-Bouligand-type structure[33,37] (shown in Fig. 2d) in which one unit consists of two adjacent lamellae forming successive orthogonal plies (marked in different colors) in helical pattern. Some other elasmoid scales like red seabream,[19] goldfish[10] and striped bass[38] have an orthogonal arrangement for their collagenous plies, whereby two adjacent lamellae are always perpendicular.

2. *Fibrillar arrangement in each lamella:* A close-up view of the assembly of collagen fibrils in one lamella, shown in Figures 2b,c, reveals that there is no grouping of fibril bundles formed

in carp scale. Each lamella is composed of isolated collagen fibrils connected by sacrificial bonds (arrows in Fig. 2c). A similar structure has been identified in most other elasmoid scales, such as arapaima,[11] red seabream,[19] tarpon,[22] goldfish[10] and striped bass.[38] This structure is different from the bundled collagen fibrils in coelacanth fish scales, shown circled with dotted lines in Figure 2e with the distinct characteristic *d*-spacing of collagen shown in Figure 2f.[33,37]

3. *Spacing between the lamella fibrils:* Similar to other elasmoid scales including arapaima, tarpon and striped bass, in the carp scale the isolated collagen fibrils in lamella are directly packed together and there is no noticeable substance between them, as shown in Figure 2b. In contrast, the space between the fiber bundles in the coelacanth scale is filled with a fibrous structure, as indicated in the inset in Figure 2e.

To further investigate the structural features of the collagenous lamellae of carp scales at the nanoscale, the internal layer was characterized by TEM; cross-sectional images are presented in Figures 3a-d. We found that there is a secondary collagenous array perpendicular to the lamellae and aligned in the thickness direction, which has not been identified in previous studies on carp scales. Figure 3a shows three adjacent collagenous lamellae of the carp scale. Secondary collagenous arrays with bifurcations are embedded in it. Thin collagen fibrils thread through the thickness of lamellae; one of them is marked with a dotted line. Detailed views in Figures 3b-d show that the threading collagen fibrils are relatively thin (d_2 ~ 20 - 40 nm), as compared to the ones in the lamella (d_1 ~ 100 nm) shown in Figure 3d, and are interspersed within the lamellae fibrils (Figs. 3c,d); they do not group with other collagen fibrils into bundles, as observed in the coelacanth scale (Figs. 3f,g). Such 2D TEM images can be projected into a 3D structure, in

which the threading secondary collagen fibrils form interfaces which partition the collagen fibrils in the lamellae, as illustrated in the schematic drawing in Figure 3e. More evidence showing that this vertical structure is not composed of single fibrils is provided in Figure S3. By comparison, the interbundle fibrils in the coelacanth scale are much more prevalent and robust (Figs. 3f,g). Indeed, with the exception of fish from the family of *Cyprinidae* and *Sarcopterygii*, all other elasmoid scales lack such through-thickness collagen fibrils. Our hypothesis is that these threading through-thickness fibrils keep the lamellae together and prevent the scale from delaminating when subjected to external bending.

Tensile Behavior of Carp Fish Scales

Based on our previous study of fish scales,[14,33] the inner collagen core is under tension when the fish scale is under attack from the penetration of a predator's teeth. Accordingly, to characterize their mechanical behavior, uniaxial tensile tests were performed on carp scales that were extracted from the mid-lateral region of a fresh carp. A representative tensile stress-strain curve is presented in Figure 4a; the insets indicate that the dog-bone shaped specimens were cut along the transverse and longitudinal directions. The stress-strain curve shown in Figure 4 is from a transverse sample. Images of the specimen during testing at successive tensile strains of ε_t = 0, 0.06, 0.11, 0.20, 0.22, 0.25, 0.27, 0.34 and 0.43 are shown in Figures 4b-j. In the linear region, the scale deformed uniformly, as shown in Figures 4b-d. Because of the greater elasticity of the collagen compared to the mineral constituents, the limiting and external layers cracked as tissue strain approached ε_t = 0.20, which was also accompanied by a small load drop on the stress-strain curve due to brittle cracking of the mineral in the external layer (as circled in Fig. 4e). With continued stretching of the collagen fibrils, at ε_t = 0.22, the external layer started to

separate partially at the relatively weak interface from the stretched collagenous lamellae (Fig. 4f), due to the modulus mismatch between the external mineralized and internal collagenous layers. At $\varepsilon_t = 0.25$, the external layer peeled off from the extreme tensile/deformed region of the collagen layer, as indicated by the dotted line in Figure 4g; this resulted in a more significant load drop. Beyond this point, the engineering stress was almost zero, although the collagen fibrils still appeared to be stretching (Fig. 4h-j) under an ultra-low sliding force, indicating that the lamellae were completely delaminated, consistent with material failure.

Figure 5 shows engineering stress-strain curves obtained from each of four conditions (seven tests per condition). The whole scale and samples without the limiting layer were tested in the longitudinal and transverse directions; the latter specimens were prepared by removing the highly mineralized limiting layer by mechanical polishing. The strength and elastic modulus in the longitudinal direction are slightly higher than in the transverse direction, although there is a much larger variation in the data for the longitudinal samples. Conversely, the total elongation tends to be smaller in the longitudinal direction. The resulting mechanical properties, specifically, the Young's modulus, ultimate tensile stress, ultimate tensile strain and total energy dissipation, are listed in Table 1.

Such modest anisotropy in the tensile properties of carp scale was also observed in arapaima scales although the property differences between orientations are more substantial.[14] Striped bass scales also exhibit in-plane anisotropic tensile behavior but the trends are different;[38] the strength in the transverse direction is higher but with a larger variation, which is opposite of the carp scales.[38] In contrast, with its double-twisted Bouligand structure, the coelacanth scale is relatively isotropic in-plane. This is because the orientations of adjacent lamellae in the double Bouligand

structure are perpendicular; the bi-layer system forms in a twisting manner, resulting in more orientations of lamellae fibrils which serves to increase isotropy. By comparison, the lamellae fibrils in the single-twisted Bouligand structure, *e.g.*, in the carp scales, only have five orientations which are equally spanned with 36˚intervals, leading to a modest anisotropic tensile behavior.

Since the superficial and highly mineralized limiting layer in the carp scale is a small fraction of the overall thickness and the mineral content of the whole scale is low, there is almost no difference between the tensile properties of the whole scale and the sample without the limiting layer. In other elasmoid scales that possess a well-defined mineral layer, such as for the coelacanth,[33] arapaima,[14] and even striped bass,[38] the inner collagenous layer (without the highly mineralized limiting layer) is stronger than the whole scale. Akin to the arapaima scale, the thicker the limiting layer (also referred to as "mineral layer" in some sources), the more significant is the difference between the mechanical properties for entire scale and the inner collagenous layer. Another factor that should not be ignored is that a minor portion of the external elasmodine (the Bouligand-type collagenous lamellae) was likely removed as well as the limiting layer. As indicated in Figure 1i, the elasmodine exhibits a gradient in mineralization with the outside being more mineralized, leading to different mechanical performance compared with the less mineralized innermost core. Since the removed external elasmodine may be inconsistent in different specimens, this could also contribute to the large variation in the tensile stress-strain curves for the samples without the limiting layer.

SEM images of the fracture surface after tensile failure of the carp scales, presented in Figure 6, show typical ductile tearing of the collagen. Since the external layer is vulnerable to peeling off

from the collagen lamellae, there is no remaining external layer on the fracture surface (Fig. 6f). Numerous straight fiber lamellae are revealed around the break region, which are due to the failure of the "sheet-like" secondary network enabling the collagenous lamella to separate. The fracture surface of relaxed broken fibers and fibrils after tensile failure (Fig. 6e) indicates their stretching during extension of the bulk specimen. In the region adjacent to the fracture, other mechanisms[13,14] can be identified, including fiber twisting, delamination, and bridging between fibrils; these are shown in Figures 6a,b,d,h. The separation between the lamellae is shown in Figure 6c, together with their delamination due to the failure of the perpendicular sheets. Further evidence of inter-lamellar separation can be seen in Figure 6g in a region behind the fracture surface; groups of dotted lines in this image delineate the orientations of four adjacent lamellae. In general, these surfaces reveal that the lamellae fibrils are significantly stretched and delaminated when inter-lamellar separation occurs.

Summarizing, the toughening mechanisms act *in concert* to dissipate the stored energy over multiple length-scales and, as such, are responsible for the excellent damage-tolerance of the carp scale. Comparing with previous studies[14,39,40], we have also confirmed that the total energy dissipation in the tensile testing of carp scale (5.83 ~ 6.80 MJ/m^3) is definitively higher than other common collagen-based materials, *e.g.,* human skin[39] (2.44 ~ 4.28 MJ/m^3), cortical bone[40] (1.8 ~ 2.5 MJ/m^3), and arapaima fish scales[14] (1.07 ~ 3.12 MJ/m^3). Such excellent toughness is conferred by a sequence of multiple-scale toughening mechanisms including the separation between external and internal layer at the macroscale, the inter-lamellar separation and fiber splitting/twisting at the mesoscale, the processes of fibrillar delamination and bridging at the

microscale, and overall the adaptive structural reorientation of the collagen in response to external loading.

In Situ Synchrotron SAXS Analysis of Toughening Mechanisms in Carp Fish Scales

Toughening by adaptive structural reorientation, whereby the majority of the fibers or fibrils rotate in order to carry more of the load, is not uncommon in collagenous materials; notable examples are in arapaima fish scales[13] and the dermis of mammals.[41] Recent studies[13,35] on the mechanical behavior of collagenous tissue show that *in situ* small-angle x-ray scattering (SAXS) is a powerful tool to precisely characterize the deformation and reorientation of collagenous lamellae under load.[42] This is attributed to the unique structure of collagen fibrils. In the collagen-based inner core of elasmoid scale, each collagen fibril is comprised of a quarter-staggered array of collagen molecules with certain amount of mineral nanoparticles filling the gap regions situated between the heads and tails of the collagen molecules, forming an alternating bands (that is, the distance between the center of two gaps); this is known as the *d*-spacing or *d*-period. When x-rays are projected onto the tissue, the collagen fibrils act as a molecular diffraction grating due to the periodicity of the collagen-mineral composite structure, generating a well-defined diffraction pattern which could be used for quantitative analysis. Figure 7a shows the experimental set-up that we used. Samples in both longitudinal and transverse directions of the scales were examined by synchrotron x-rays during tension testing with a series of two-dimensional SAXS patterns obtained, as shown in Figures 7c,d. The dark blue rectangular mesh in the SAXS pattern is due to the space between the modules of the Pilatus detector. Representative SAXS patterns generated by our unloaded longitudinal samples are shown in Figure 7c. The interaction of the x-rays with collagenous lamellae creates several sets

of concentric arcs in the diffraction pattern. Based on Bragg's law, the distance between the beam center and the first-order arc is the reciprocal of the *d*-spacing of collagen fibrils (Figure 7b), which is 63.2 ± 1.1 nm in our carp scale specimens. A detailed explanation of this reciprocal relationship is provided in the Supplementary Information (Fig. S6). Based on the change in this distance in each diffraction pattern, the elastic strain in the collagen fibrils can be quantified. The azimuthal angle of the arcs, referred to as Ψ, indicates one distinct orientation of the collagen fibrils, as illustrated in Figure 7b. The deformation of the collagen fibrils under uniaxial tension loading ($\Psi = 0°$) can be quantitively analyzed for the sequence of the SAXS pattern. Further details about the analysis are provided below.

Figure 7d shows a typical tensile stress-strain curve with five SAXS patterns revealing the deformation of the collagen fibrils under loading at tissue strains ε_t of 0, 0.06, 0.10, 0.14 and 0.18. A close-up view of the first-order Debye-Scherrer ring coupled with the real-time pictures at the initial state ($\varepsilon_t = 0$) and fully stressed state ($\varepsilon_t = 0.18$) are provided in the insets. When the scale is fully relaxed, the diffraction pattern is composed of round arcs with some preferred orientations. As the applied tensile load increases, the diffraction pattern evolves accordingly. When the tensile stress reaches its maximum at $\varepsilon_t = 0.18$, the specimen is fully stretched, and the diffraction pattern changes from round shape (before tension) to a 'hexagon-like' shape at the maximum stress, indicating significant anisotropic strains in the structural evolution of the inner lamellae layer.

Reorientation of the collagen fibrils under load: To quantify the real-time reorientation of the collagen fibrils, plots of intensity *vs*. azimuthal angle (orientation of the collagen fibrils) at five strains 0, 0.06, 0.10, 0.14 and 0.18 during tension testing were generated from the 2D SAXS

pattern, as shown in Figure 8a. The data on the fractured sample at a strain of 0.22 were also included. Prior to testing (at $\varepsilon_t = 0$), the single Bouligand structure of the carp scale showed highly oriented collagen fibrils with an included angle of ~36° as the high intensity peaks (-78°, -46°, - 9°, 27°, 61°) indicate in the plot ($\varepsilon_t = 0$) in Figure 8a. This unique twisting angle is very consistent in this single-twisted Bouligand structure, which was confirmed by investigation of several specimens (Fig. S4). As the applied load is increased, the collagen fibrils at large angles (*i.e.*, Ψ = -78°, 61°) reorient further away from the loading direction with increasing intensity (shown by arrows); several peaks (dotted circles) appearing at the angles of -65°~ -55° reveal that the collagen lamellae reorient towards, and delaminate along, that orientation. As the loading is increased, lamellae at angles closer to the loading direction (Ψ = - 9° to Ψ = 27°) reorient and distribute over a broad range (between -40° and 40°) towards the loading direction (shown by the stars and triangles in Fig. 8a). After the scale is broken (at $\varepsilon_t = 0.22$), the peaks reappear but at more orientations than in the original state, indicating that a significant portion of the lamellae have reoriented, *i.e.*, the scale has experienced significant permanent deformation and the collagenous lamellae are no longer oriented with an specific included angle of 36°.

Compared to the single Bouligand structure of carp fish scales, the toughening mechanisms in the double Bouligand structure of the coelacanth fish scale are simpler, as shown for comparison in Figure 8b. Since the structure is formed by orthogonal bilayers twisted in a Bouligand pattern, collagen lamellae are aligned in more orientations with no clear intensity peaks. As the load increases, collagen fibrils ranging between Ψ = - 60° and Ψ = 40° gradually rotate towards the loading direction (shown by arrows at 0°) due to interfibrillar sliding in response to the shear stresses; the ones at large angles (-90° < Ψ < -60°, 40° < Ψ < 90°) rotate away from the loading

direction and delaminate/separate significantly (shown by a lower intensity). By rotating toward the loading direction, the projected length of the fibrils increases. This rotation has an analogy in the plastic deformation by single slip of metallic monocrystals. This mechanism was explained and quantified by Yang *et al.*[14] for the arapaima scales and modeled by molecular dynamics. On the other hand, the rotation away from the direction of loading, for fibrils oriented at large angles to it, can be explained by separation of the fibrils in the lamellae produced by tension. This creates curved fibrils with varying angles to the tensile axis.

Quantification of the deformation of lamellae of collagen fibrils: For the determination of the fibrillar strains, the diffraction circles were evenly divided into 17 sectors with a span of 10° from $\Psi = -90°$ to $\Psi = 70°$ and the average radius r of each sector was calculated. The radius r is inversely proportional to the characteristic d-spacing through Bragg's law, and thus the d-spacing of the collagen fibrils in each sector was obtained. The change in d-spacing in each sector was then divided by the initial, unstressed d-spacing of d_0 to define the collagen fibril strain ε_f^{Ψ}. The strains are plotted as a function of the azimuthal angle in Figure 9a. Calculations were performed for the five externally imparted strain levels (tissue strains) during tensile deformation: 0, 0.06, 0.10, 0.14, 0.18, and 0.22 (at failure). For comparison, a similar plot for the coelacanth scale is presented in Figure 9b.[33]

Figure 9a shows that the imparted tissue strain results in tensile fibrillar strains for small angles ($-40° < \Psi < 40°$). This is most pronounced for $\Psi = 0°$ and 10° and increases with tissue strain. However, the fibrillar strain is significantly lower (by approximately one half) than the tissue strain by virtue of interfibrillar sliding. The maximum tensile fibril strain, when the tissue is fully stretched, is about 0.1; this is considerably lower than the global tissue strain, 0.18, indicating

that significant fibrillar sliding has taken place. The same mechanism was also identified in both coelacanth and arapaima scales; however, the fibril extensibility of carp scale (ε_f ~ 0.08) is higher than that of the arapaima scale (ε_f ~ 0.05),[13] but lower than the coelacanth's scale (ε_f ~ 0.12).[33] A similar effect also exists in rabbit dermis.[41] Such sliding between collagen fibrils in these collagenous tissues, *e.g.*, fish scales and mammal dermis, is permanent.[13,33,41]

For the lamellae oriented at large angles (- 90° < Ψ < - 40° and 40° < Ψ < 90°), shown in Figure 9a, the fibrils are compressed. This reduction in length is associated with the tensile stretching of the lamellae at small angles Ψ with the tensile direction. These lamellae exhibit a reduction in their lateral dimensions due to a Poisson's ratio effect. This reduction in the lateral dimension causes a compression in the lamellae at large angles, which are connected to them. Thus, negative strains are apparent, shown in Figure 9a, for Ψ between ±40° and ± 90°. This unique deformation mechanism for carp scales is also confirmed by measurements made on several specimens, along different directions, as illustrated in Figure S5.

These SAXS results and their analysis, presented in Figures 8 and 9, can be summarized in the schematic drawing in Figure 10, which shows the sequence of mechanisms experienced by the collagenous lamellae in the carp scale based on both lamellar reorientation (quantified in Fig. 8a) and deformation (Fig. 9a). The first stage during tensile loading is the cracking and peeling off of the highly mineralized external layer (Fig. 10a), which is confirmed by our observations in Figures 4e-g. The lamellae with orientations close to the loading axis (- 40° < Ψ < 40°) are subjected to tensile strains, resulting in an increase in length with increasing *d*-spacing ($d > d_0$, Figs. 10b,c) and reorient towards the loading direction by interfibrillar shear (Fig. 10c). These mechanisms, which are proposed based on our analysis of the SAXS experiments (from Figs. 8a

and 9a), are confirmed by our observations on the fracture surface of the tensile specimens presented in Figure 6, which specifically show fibrillar shearing and delamination (Fig. 6a) and relaxation of stretched fibers after tensile failure (Fig. 6e). There is some difference in the fibrillar strain distribution between the carp and coelacanth scale, shown in Figures 9a,b. Since the threading fibrils in carp scale are not as profuse as the ones in coelacanth scale, the lamellae are more vulnerable to failure by delamination as illustrated in Figure 10d. This delamination is characterized by SEM in Figures 6b,c. Interestingly, a transitional range exists where the fibril deformation changes from tension to compression, *i.e.*, the fibrils initially oriented from- 40° to -30° and from 40° to 50° ($d < d_0$, Fig. 10d). This indicates that deformation takes place exclusively by shear on some fibrils within these two ranges. The fibrils strained at $\varepsilon_t = 0.22$, when the tissue completely breaks, do not recover their original value ($\varepsilon_t = 0$), indicating the retention of tensile and compressive plastic deformation when the scale is stretched to fracture. Such plastic deformation is also evident on the ductile fracture surfaces shown in Figures 4j and 6a.

By combining this sequence of deformation mechanisms discussed above, the Bouligand-type lamellar inner base of the carp scale adapts to the applied load by lamellar rotation, fibrillar deformation and sliding, and interlayer separation, as illustrated in Figure 10e, and as such is capable of dissipating stored elastic energy effectively and conferring to the carp scale its excellent toughness.

CONCLUSIONS

We have characterized the detailed structure of the modern elasmoid scales of the common carp and determined their mechanical properties. Using synchrotron small-angle x-ray scattering, the

lamellar rotation and fibril deformation have been quantified in order to identify the salient toughening mechanisms. To improve our understanding of the prevailing mechanisms, we have further compared our results for the carp scale with those of the primitive elasmoid scales from the coelacanth. Based on this work, several conclusions on the prime structural components of this damage-tolerant natural material can be made:

- With respect to the structure of carp scales, the external layer is composed of highly mineralized woven fibrils covered by an extremely thin and discontinuous mineral layer. The inner core is a highly ordered "plywood-like" structure, consisting of superimposed collagenous lamellae, successively rotated by 36° to form a typical single-twisted *Bouligand* structure. The small amount of secondary 'threading' fibrils along the thickness direction is presumed to ensure the integrity of the scales.
- The tensile behavior of the carp scale, which represents the behavior of the inner collagenous layer under penetration (*i.e.*, from attack by a predator), was found to have higher strength and toughness (by ~20%) in the longitudinal, as compared to the transverse, direction. A synergy of toughening mechanisms including external layer separation, inter-lamellae separation, fiber twisting and splitting, fibrillar delamination and bridging, and fibrillar reorientation, all act *in concert* to improve the damage tolerance of the scales.
- *In situ* SAXS measurements during mechanical straining of the carp fish scales demonstrate adaptive structural reorientation, in that the lamellae oriented closer to the tensile direction rotate towards it to carry more load while stretched and the ones oriented far from the loading direction rotate away from it while compressed. However, the collagen fibrils present two local maxima strains at azimuthal angles of Ψ = - 20° and Ψ = 10° to the tensile axis.

Compared to the single Bouligand structure of carp, the double Bouligand structure containing the secondary "threading" bundles of the coelacanth fish scales exhibits higher integrity so that the collagen fibrils reach to one clear maximum fibrillar tension strain under load.

- These deformation mechanisms operate together to render the carp scale an excellent dermal armor, and may well provide further inspiration for the design advanced synthetic structural materials with unprecedented toughness and penetration resistance.

EXPERIMENTAL PROCEDURES

Resource Availability

Lead Contact

Further information and requests for resources and reagents should be directed to and will be fulfilled by the Lead Contact, Robert O. Ritchie (roritchie@lbl.gov)

Materials Availability

The scale samples were collected from a common carp (*Cyprinus carpio*) fish with a size of 670 mm, which was purchased from Ranch 99 Market (7330 Clairemont Mesa Blvd, San Diego, CA, USA). The scales were extracted from their pockets with tweezers and preserved in deionized water. They varied from 20 to 40 mm in length but the ones that we used were all ~30 mm in length and extracted from the mid-lateral region. For comparison, coelacanth scales were obtained from a *Latimeria chalumnae* with a length of 950 mm in the Marine Vertebrate Collection of Scripps Institution of Oceanography, University of California, San Diego; the specimen was preserved in 80% isopropanol since it was collected from the Grand Comore Island in 1973. They were peeled off from the *linea lateralis* below the anterior dorsal fin.

Structural Characterization

The structure of the scales and the fracture surfaces after tensile testing were all characterized in a FEI Quanta 250 and FEI Apero scanning electron microscope (SEM; FEI, Hillsboro, OR). To obtain oblique fracture surfaces, scales were immersed in liquid nitrogen for 30 s and immediately fractured using forceps. The samples were first immersed in the 2.5% glutaraldehyde for 1 h to fix the structure and then dehydrated with an ascending series of ethanols (30, 50, 70, 90, 95 and 100 vol.% twice), before being dried using an automatic critical point dryer (Tousimis AutoSamdri 815A, MD). All dried samples were then sputter coated with iridium using an Emitech K575X sputter coater (Quorum Technologies Ltd.) before observation. TEM images were taken on FEI Technai 12 (Spirit, 120-kV) transmission electron microscope (FEI, Hillsboro, OR).

Preparation of TEM Specimens

The carp and coelacanth scales were first cut into small strips, with a length of 5 mm and a width of 2 mm, and then immersed into 2.5% glutaraldehyde in 0.15 M sodium cacodylate buffer (pH 7.4) for 1 h to fix the structure. The fixed specimens were stained with 1% OsO_4 solution with 8% potassium ferrocyanide in 0.5 M sodium cacodylate buffer for overnight at room temperature. The scales were then stained with 2% aqueous uranyl acetate for 12 h and subsequently dehydrated with an ascending ethanol series (50, 70, 90, 100% twice), followed by a 1:1 ratio of 100% ethanol and 100% acetone, and finally 100% acetone. The fully dehydrated specimens were embedded in Spurr's low viscosity resin and polymerized at 60°C for 72 h. The obtained blocks were then sectioned parallel to the vertical cross-section before ultrathin slices with thickness of ~80 nm were generated using a Leica Ultracut UCT ultramicrotome (Leica)

and a Diatome diamond knife (Diatome). Ultramicrotomed sections were then placed on copper grids for TEM observation and post stained with Sato lead for 1 min before final examination.

Uniaxial Tensile Testing

Dog-bone shaped tensile specimens of carp scales with dimensions of 20 × 3 mm were cut along longitudinal and transverse directions from carp scales with a thickness of between 0.2 and 0.3 mm. The outer layers of some samples were removed using silicon carbide polishing paper of 180 # - 2500 #, leading to final thickness of ~0.1 mm. To prevent sliding during tensile testing, the ends of the samples were glued between sand paper sheets using cyanoacrylate glue, resulting in a gauge length of ~10 mm. Uniaxial tensile tests were performed on an Instron 3342 mechanical testing machine (Instron Corp., Norwich, MA) with a load cell of 500 N at a strain rate of 10^{-3} s^{-1}; samples were tested immediately after being removed from deionized water, where they had been kept prior to testing. Values of Young's modulus were estimated by linear fitting the stress-strain curve at the early stage of the tensile testing (in the linear portion). We also determined the ultimate tensile stress, uniform elongation (strain at maximum stress) and the toughness, the latter being measured in terms of the area beneath the uniaxial stress-strain curves.

***In Situ* Small-Angle X-Ray Scattering (SAXS) During Mechanical Testing**

Using identical specimen preparation procedures as for the uniaxial tensile tests, specimens for *in situ* SAXS measurements were cut in both longitudinal and transverse directions from complete carp scales after the mineral layer had been removed. The resulting specimens were loaded in tension, while simultaneously exposing them to synchrotron x-rays at beamline 7.3.3 at the Advanced Light Source synchrotron radiation facility (Lawrence Berkeley National Laboratory, Berkeley, CA, USA). The tensile tests were performed using a Linkam TST-350 tensile stage

(Linkam Scientific Instruments) with a 200N capacity load cell to measure the force. Such an experimental set-up allows for SAXS data collection to be recorded in real time with the measurement of the load–displacement curve. The mechanical tests were performed at room temperature and a strain rate of 1.0×10^{-3} s^{-1}.

During mechanical testing, a high flux of synchrotron x-rays was focused on the tensile specimen and scattered by the periodicity of the collagenous lamellae, which in essence serves as a macroscopic strain gauge; this generates a diffraction pattern composed of several concentric arcs on the screen, shown in (Fig. 7b). In each set of concentric arcs, the arc closest to the beam center (the first-order arc) represents the distance q from the beam center which has a reciprocal relationship with the d-spacing of the collagen fibrils, whereas the rest of the concentric arcs are higher order arcs, corresponding to the harmonics of this d-period. The azimuthal angle of each set of arcs, referred to as Ψ, indicates one distinct orientation of the collagen fibrils in the scale, as illustrated in the inset of in Figure 7b. Uniaxial tensile loading was applied along the $\Psi = 0°$ direction, Therefore, the change of in the value of Ψ q and q Ψ for all sets of the first-order arcs at different tissue strains can quantify, respectively, the rotation of the collagenous lamellae and the deformation of strain in the collagen fibrils in real time during uniaxial tensile extension.

A Pilatus3 2M detector (Dectris Ltd., Baden, Switzerland) was used to collect the SAXS data. The detector was located at the largest allowable distance, around 4 m, to detect fine changes in the position of the collagen peaks. The sample was exposed to x-rays for 0.5 s with intervals of ~5 s during the mechanical test; this radiation dosage was sufficiently low so as not to affect the structure and properties of the scales.

Quantification of fibril orientation using SAXS: On examining the SAXS spectra patterns, 360 of even sectors were made on the Debye-Scherrer rings with a span of 1°, starting from $\Psi = 0°$ to $\Psi = 360°$; as such, a sector graph was generated by the polar transformation of the 2-D diffraction pattern using the software IGOR Pro (Wavemetrics) in conjunction with the custom macro NIKA (Jan Ilavsky, Argonne National Laboratory, IL, USA). Based on the obtained square map of intensity *vs*. pixel, the 1-D graphs, specifically the plots of the integrated intensity as a function of azimuthal angle, were created by using the 'Image line profile' tool in NIKA.

Quantification of fibril strains: The strains in the collagen fibrils were measured from the x-ray data in terms of the change in 1-D peak position determined from the plot of integrated diffraction intensity as a function of *d*-spacing. By using the same software as in the quantification of fibril orientation, the sample detector distance and beam center were calibrated with the 2-D diffraction pattern of a silver behenate standard. In order to convert the 2-D SAXS data into 1-D peaks, 17 sectors were evenly made on the upper half of the Debye-Scherrer rings, starting from $\Psi = -5°$ to $\Psi = 165°$, with a span of 10° in each sector; then the integrated intensity over the diffraction arc in each sector was radially averaged to obtain the relationship between the intensity peaks and the radial distance of the arc, q. Based on the numerical relationship between q and the d-spacing, plots of integrated intensity as a function of the d-spacing for all 17 sectors were generated by the software; intensity peaks were fit to an exponential Gaussian function and a linear background to precisely locate the peak positions. The strain in the collagen fibrils was measured as the change in position of the center of the first-order collagen peak, normalized by the unstressed state.

Data and Code Availability

Data supporting the findings of this paper are available from the corresponding authors upon reasonable request.

SUPPLEMENTAL INFORMATION

Supplemental information can be found online at https://doi.org/10.1016/j.matt.....

ACKNOWLEDGMENTS

This work was supported by a Multi-University Research Initiative through the Air Force Office of Scientific Research (AFOSR-FA9550-15-1-0009) via subcontracts to the University of California in San Diego and Berkeley. We acknowledge the use of beam line 7.3.3 at the Advanced Light Source at the Lawrence Berkeley National Laboratory, which is supported by the Office of Science, Office of Basic Energy Sciences, Division of Materials Sciences and Engineering of the U.S. Department of Energy under Contract no. DE-AC02-05CH11231. We also thank Mason Mackey for help in preparing the TEM samples and Guillaume Castillon for his help with the TEM image processing. TEM characterization was carried out using shared research resources at the National Center for Microscopy and Imaging Research (NCMIR) at UCSD supported by the NIH under award number P41 GM103412 (M.H. Ellisman). Thanks are also due to Zixiang Tang for preparing some of the schematic drawings.

AUTHORS CONTRIBUTIONS

Conceptualization H.Q., W.Y., M.A.M and R.O.R; Methodology, H.Q., W.Y., E.S., M.A.M and R.O.R; Investigation, H.Q., M.L., W.Y. and E.S.; Writing – Original Draft, H.Q., W.Y., M.A.M and R.O.R; Writing – Review & Editing, H.Q., W.Y., E.S., M.A.M and R.O.R; Funding Acquisition, M.A.M and R.O.R; Resources, M.A.M and R.O.R; Supervision, M.A.M and R.O.R.

DECLARATION OF INTERESTS

The authors declare no competing interests.

REFERENCES

1. Sire, J. Y., Donoghue, P. C. J., and Vickaryous, M. K. (2009). Origin and evolution of the integumentary skeleton in non-tetrapod vertebrates. J. Anat. 214(4), 409-440.
2. Wang, B., Yang, W. McKittrick, J., and Meyers, M. A. (2016). Keratin: Structure, mechanical properties, occurrence in biological organisms, and efforts at bioinspiration. Prog. Mater. Sci. 76, 229-318.
3. Liu, Z., Zhang, Z., Ritchie, R. O. (2018). On the materials science of Nature's arms race. Adv. Mater. 30(32),1705220.
4. Yang, W., Chen, I. H., Gludovatz, B., Zimmermann, E. A., Ritchie, R. O., and Meyers, M. A. (2013). Natural flexible dermal armor. Adv. Mater. 25(1), 31-48.
5. Abrams, P. A. (2000). The evolution of predator-prey interactions: Theory and evidence. Ann. Rev. Ecology Systematics 31, 79-105.
6. Bruet, B. J. F., Song, J. H., Boyce, M. C., and Ortiz, C. (2008). Materials design principles of ancient fish armour. Nature Mater. 7(9), 748-756.
7. Yang, W., Gludovatz, B., Zimmermann, E. A., Bale, H. A., Ritchie, R. O., and Meyers M. A. (2013). Structure and fracture resistance of alligator gar (Atractosteus spatula) armored fish scales. Acta Biomater. 9(4), 5876-5889.
8. François, J. M. (1984). Spatial organization and mineralization of the basal plate of elasmoid scales in osteichthyans. Structure and fracture resistance of alligator gar (Atractosteus spatula) armored fish scales. Amer. Zoolog. 24(4), 953-964.
9. Sire, J.-Y., Huysseune, A. (2003). Formation of dermal skeletal and dental tissues in fish: a comparative and evolutionary approach. Biolog. Rev. 78(2), 219-249.
10. Onozato, H., and Watabe, N. (1979). Studies on fish scale formation and resorption. Cell Tissue Res. 201(3), 409-422.
11. Lin, Y. S., Wei, C. T., Olevsky, E. A., and Meyers, M. A. (2011). Mechanical properties and the laminate structure of Arapaima gigas scales., J. Mech. Behav. Biomed. Mater. 4(7),1145-1156.
12. Meyers, M. A., Lin, Y. S., Olevsky, E. A., and Chen, P. Y. (2012). Battle in the Amazon: Arapaima versus piranha., Adv. Eng. Mater. 14(5), B279-B288.

13. Zimmermann, E. A., Gludovatz, B., Schaible, E., Dave, N. K. N., Yang, W., Meyers, M. A., and Ritchie, R. O. (2013). Mechanical adaptability of the Bouligand-type structure in natural dermal armour. Nature Comm. 4, 2634.

14. Yang, W., Sherman, V. R., Gludovatz, B., Mackey, M., Zimmermann, E. A., Chang, E. H., Schaible, E., Qin, Z., Buehle, M. J. r, Ritchie, R. O., and Meyers, M. A. (2014). Protective role of Arapaima gigas fish scales: structure and mechanical behavior. Acta Biomater. 10(8), 3599-3614.

15. Torres, F. G., Troncoso, O. P., Nakamatsu, J., Grande, C. J., and Gómez, C.M. (2008). Characterization of the nanocomposite laminate structure occurring in fish scales from Arapaima Gigas. Mater. Sci. Eng. C 28(8), 1276-1283.

16. Chen, P. Y., Schirer, J., Simpson, A., Nay, R., Lin, Y. S., Yang, W., Lopez, M. I., Li, J. A., Olevsky, E. A., and Meyers, M. A. (2012). Predation versus protection: Fish teeth and scales evaluated by nanoindentation. J. Mater. Res. 27(1), 100-112.

17. Torres, F. G., Bourhis, E. Le, Troncoso, O. P., and Llamoza, J. (2014). Structure-property relationships in arapaima gigas scales revealed by nanoindentation tests. Polymer Compos. 22(4), 369-374.

18. Torres, F. G., Malásquez, M., and Troncoso, O. P. (2015). Impact and fracture analysis of fish scales from Arapaima gigas. Mater. Sci. Eng. C 51, 153-157.

19. Ikoma, T., Kobayashi, H., Tanaka, J., Walsh, D., and Mann, S. (2003). Microstructure, mechanical, and biomimetic properties of fish scales from Pagrus major. J. Struct Biol. 142(3), 327-333.

20. Zhu, D. J., Szewciw, L., Vernerey, F., and Barthelat, F. (2013). Puncture resistance of the scaled skin from striped bass: Collective mechanisms and inspiration for new flexible armor designs. J. Mech. Beh. Biomed. Mater. 24, 30-40.

21. Dastjerdi, A. K., and Barthelat, F. (2015). Teleost fish scales amongst the toughest collagenous materials. J. Mech. Beh. Biomed. Mater. 52, 95-107.

22. Gil-Duran S., Arola, D., and Ossa, E. A. (2016). Effect of chemical composition and microstructure on the mechanical behavior of fish scales from Megalops Atlanticus. J. Mech. Beh. Biomed. Mater. 56, 134-145.

23. Meyers, M. A., McKittrick, J., and Chen P. Y. (2013). Structural biological materials: critical mechanics-materials connections. Science 339(6121), 773-779.

24. Ritchie, R. O. (2011). The conflicts between strength and toughness. Nature Mater. 10(11), 817-822.

25. Wakeling, J. M., Kemp, K. M., and Johnston, I. A. (1999). The biomechanics of fast-starts during ontogeny in the common carp cyprinus carpio. J. Exp. Biology 202(22), 3057-3067.

26. Arola, D., Murcia, S., Stossel, M., Pahuja, R., Linley, T., Devaraj, A., Ramulu, M., Ossa, E. A., and Wang J. (2018). The limiting layer of fish scales: Structure and properties. Acta Biomater. 67, 319-330.

27. Marino Cugno Garrano, A., La Rosa, G., Zhang, D., Niu, L. N., Tay, F. R., Majd, H., and Arola, D.(2012). On the mechanical behavior of scales from Cyprinus carpio. J. Mech. Beh. Biomed. Mater. 2012, 7, 17-29.

28. Bonwick, G. A., Witcomb, D. M., Davies, D. H., and Winstanley, S. (1989). Scale surface micro-structures of British freshwater cyprinidae. Micron Microscopica Acta 20(3), 247-253.

29. Esmaeili, H. R., and Gholami, Z. (2011). Scanning electron microscopy of the scale morphology in cyprinid fish, Rutilus frisii kutum Kamenskii, 1901 (Actinopterygii: Cyprinidae). Iranian J. Fisheries Sci. 10(1), 155-166.

30. Liu, P., Zhu, D., Wang, J., and Bui, T. Q. (2017). Structure, mechanical behavior and puncture resistance of grass carp scales. J. Bionic Engin. 14(2), 356-368.

31. Murcia, S., McConville, M., Li, G., Ossa, A., and Arola, D. (2015). Temperature effects on the fracture resistance of scales from Cyprinus carpio. Acta Biomater. 14, 154-163.

32. Browning, A., Ortiz, C., and Boyce, M. C. (2013). Mechanics of composite elasmoid fish scale assemblies and their bioinspired analogues. J. Mech. Beh. Biomed. Mater. 19, 75-86.

33. Quan, H., Yang, W., Schaible, E., Ritchie, R. O., and Meyers, M. A. (2018). Novel defense mechanisms in the armor of the scales of the “living fossil” coelacanth fish. Adv. Funct. Mater. 28(46), 1804237.

34. Meunier, F. J., Cupello, C., and Clément, G. (2019). The skeleton and the mineralized tissues of the living coelacanths. Bulletin of Kitakyushu Museum of Natural History and Human History. 17, 37-48.

35. Sire, J.Y., Quilhac, A., Bourguignon, J., and Allizard, F. (1997). Evidence for participation of the epidermis in the deposition of superficial layer of scales in zebrafish (Danio rerio): A SEM and TEM study. J. Morphol. 231(2), 161-174.

36. Martini, R., and Barthelat, F. (2016). Stability of hard plates on soft substrates and application to the design of bioinspired segmented armor. J. Mechan. Phys. Solids, 92, 195-209.

37. Giraud, M.M., Castanet, J., Meunier, F.J., and Bouligand, Y. (1978). The fibrous structure of coelacanth scales: a twisted 'plywood'. Tissue Cell 10(4), 671-686.

38. Zhu, D., Ortega, C.F., Motamedi, R., Szewciw, L., Vernerey, F., and Barthelat F. (2012). Structure and mechanical performance of a “modern” fish scale. Adv. Eng. Mater. 14(4), B185-B194.

39. Annaidh, A. N., Bruyère, K., Destrade, M., Gilchrist, M. and Otténio, M. (2012). Characterization of the anisotropic mechanical properties of excised human skin. J. Mech. Behav. Biomed. Mater., 5 (1), 139-148.

40. Wang, X. and Nyman, J. S. (2007). A novel approach to assess post-yield energy dissipation of bone in tension. J. Biomech. 40 (3), 674-677.

41. Yang, W., Sherman, V. R., Gludovatz, B., Schaible, E., Stewart, P., Ritchie, R. O., and Meyers, M. A. (2015). On the tear resistance of skin. Nature Comm., 6, 6649.

42. Hexemer, A., Hexemer, A., Bras, W., Glossinger, J., Schaible, E., Gann, E., Kirian, R., MacDowell, A., Church, M., Rude, B., Padmore, H. (2010). A SAXS/WAXS/GISAXS beamline with multilayer monochromator. J. Phys. Conf. Ser. 247 (2010) 012007.

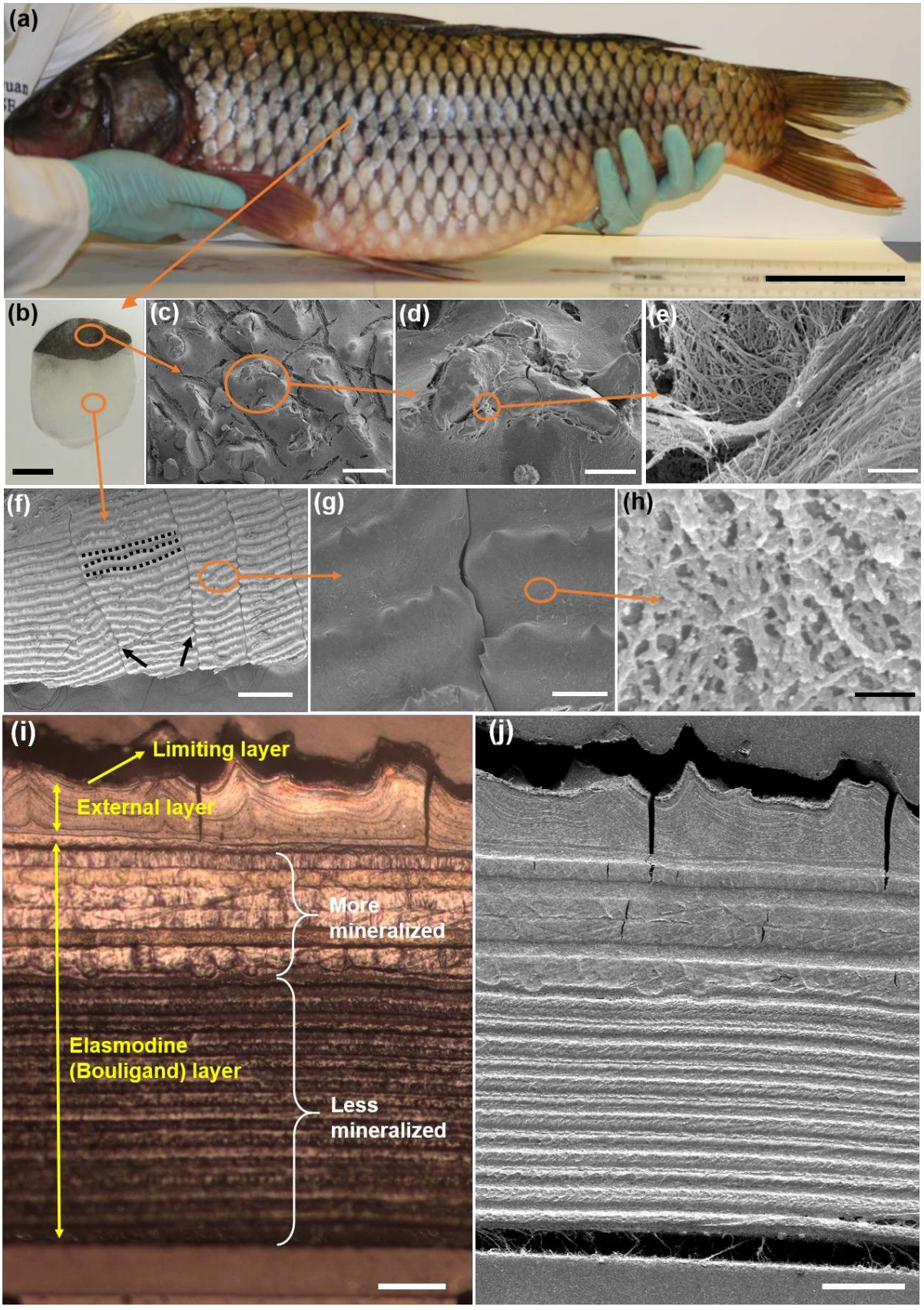
(a)
(b)
(c)
(d)
(e)
(f)
(g)
(h)
(i)
Limiting layer
External layer
More mineralized
Elasmodine (Bouligand) layer
Less mineralized
(j)

Figure 1 | Surface morphology and the multilayered structure of carp scales. (**a**) The common carp (*Cyprinus carpio*) from which the scales are extracted. Scale bar, 100 mm. (**b**) The carp scale is a typical elasmoid scale with an oval shape; two thirds of surface (the white part) are overlapped by neighboring scales. Scale bar, 10 mm. (**c-h**) Scanning electron micrographs of the outer surface of the carp scale. (**c**) The mineralized denticles are scattered on the exposed part (dark region) and increase the surface roughness. Scale bar, 200 μm. (**d**) Most parts of the denticle are covered by the dermis and only the rounded tip is exposed. Scale bar, 50 μm. (**e**) The fibrous dermis tissue around the denticle tip. Scale bar, 1 μm. (**f**) The overlapped region of the carp scale suggests that the mineral ridges (*circuli*), indicated as dotted lines, are interrupted by cracks (*radii*), as indicated by arrows. Scale bar, 200 μm. (**g**) A close-up view reveals that the mineral ridges which define the *circuli* are regularly spaced. Scale bar, 20 μm. (**h**) The external layer, which is composed of woven mineralized fibrils (diameter ~30 to 50 nm), is exposed at the spaces between the ridges. Scale bar, 200 nm. (i) Optical microscopy image of the cross-section of a carp scale. It clearly shows that the scales have a multilayered structure: the limiting layer, external layer and elasmodine (Bouligand) layer. The outer elasmodine layer is more mineralized than the inner. Scale bar, 50 μm. (g) Scanning electron micrographs (SEM) of the region shown in (i). Scale bar, 50 μm.

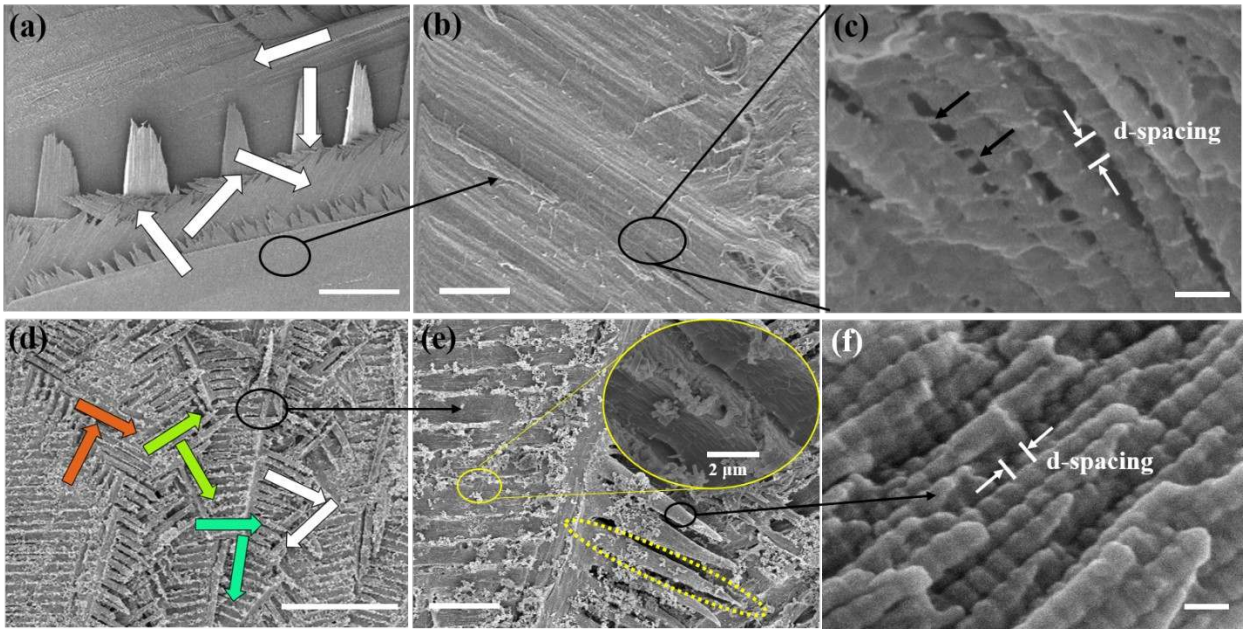

Figure 2 | The Bouligand-type collagenous lamellae of the carp, as compared to coelacanth, scales. (**a**-**c**) The carp scale. (**a**) Freeze fracture of carp scale reveals the layered twisted plywood structure of the inner layer. The arrows represent the orientations of each collagenous lamella, indicating their periodic alignments; there are 5 orientations in each period (Layer 1 and Layer 6 are oriented at same direction). Scale bar, 100 μm. (**b**) Absence of distinct fiber bundles in carp scale. Each lamella is composed of parallel collagen fibrils without gap. Scale bar, 20 μm. (**c**) High magnification of (b) shows the characteristic band pattern of collagen fibrils and the sacrificial bonding connecting the fibrils, as indicated by the arrows. Scale bar, 100 nm. (**d**-**f**) The coelacanth scale. (**d**) The inner layer of coelacanth scale also has a laminated structure, but the arrangement of lamellae orientation is different. Two adjacent layers are almost perpendicular to each other (1&2; 3&4…) and the bi-layers form a twisted Bouligand pattern. Scale bar, 50 μm. (**e**) The collagen fibrils form distinct bundles circled by the dotted line and the space between bundles is filled by out-of-plane fibrils, as shown in the magnified inset. Scale bar, 10 μm. (**f**) A high magnification image shows the well-defined band (*d*-spacing) pattern of the collagen fibrils. Scale bar, 100 nm.

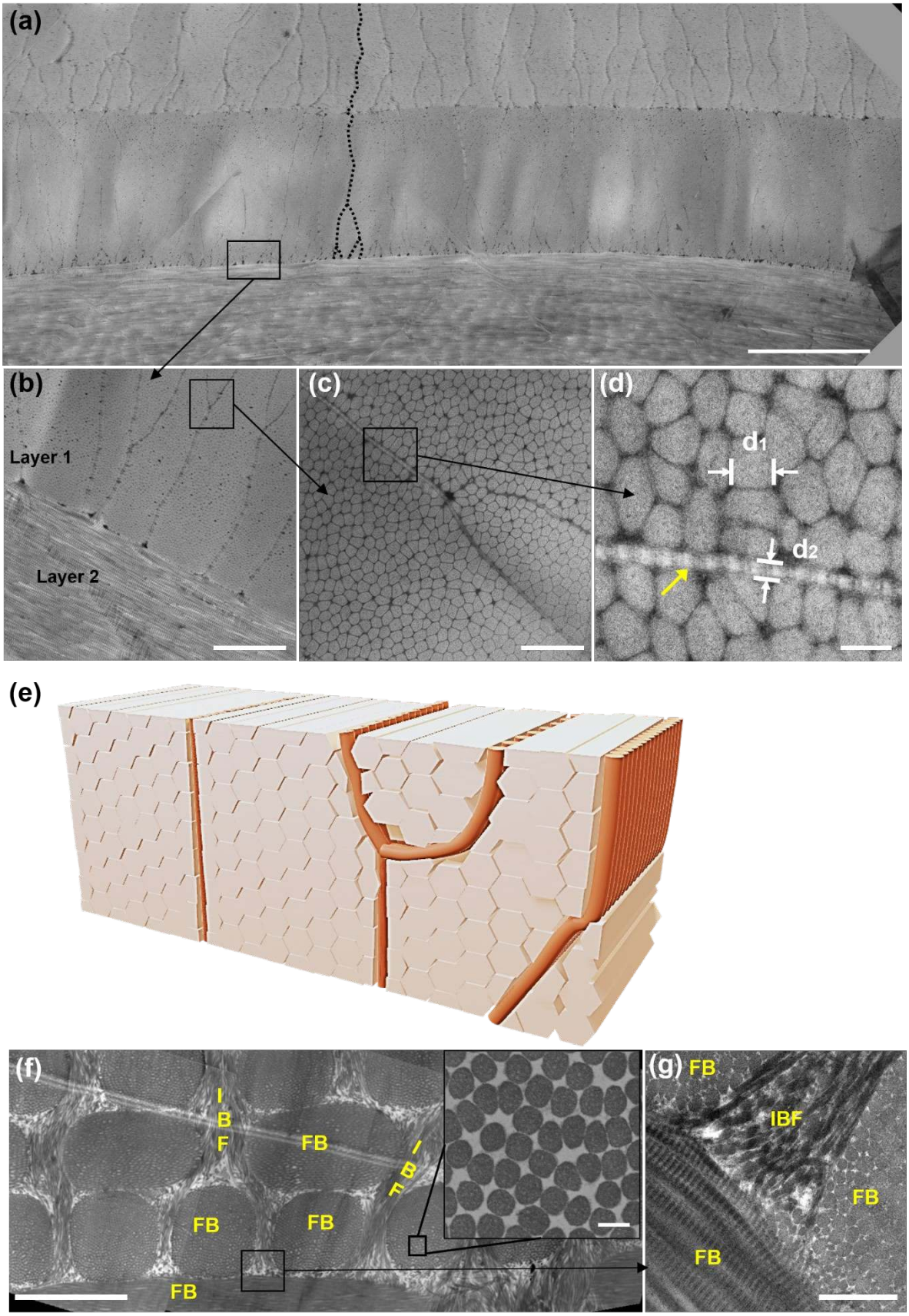
(a)
(b)
Layer 1
Layer 2
(c)
(d)
d1
d2
(e)
(f)
I
B
F
FB
I
B
F
FB
FB
FB
(g) FB
IBF
FB
FB

Figure 3 | The secondary fibrous frame in the carp and coelacanth scales. (**a**-**d**) Transmission electron micrographs (TEMs) of carp scale with different magnifications. (**a**)The cross-section of three neighboring layers indicates there are a few very thin vertical fibrils going through the thickness direction. One of them is marked with dotted line. Scale bar, 10 μm. (**b**) Higher magnification image of the junction between two layers 1 and 2. Scale bar, 2 μm. (**c**) Close-up view of the cross-section reveals the delamination of the vertical fibril and that the collagen fibrils which comprise the lamella are tightly packed and squeezed into a polygonal shape. Scale bar, 500 nm. (**d**) High magnification image shows that the thin vertical fibril is collagen, as indicated by the arrow. The diameter of the lamellar and vertical fibrils is denoted as d_1 and d_2, respectively. Scale bar, 100 nm. (**e**) Schematic illustration of the structure of the vertical fibrils interspersed in the lamellae. (**f**,**g**) TEM of a coelacanth scale. The space between the fiber bundles (FBs) are filled with abundant interbundle fibrils (IBFs) which form a well-defined matrix to hold the Bouligand-type lamella. Scale bar, 5 μm and 500 nm, respectively. The inset in (**f**) shows that the packing of the fibrils in the fiber bundle is not as tight as that in carp scales and their cross-sections remain round shape. Scale bar, 100 nm.

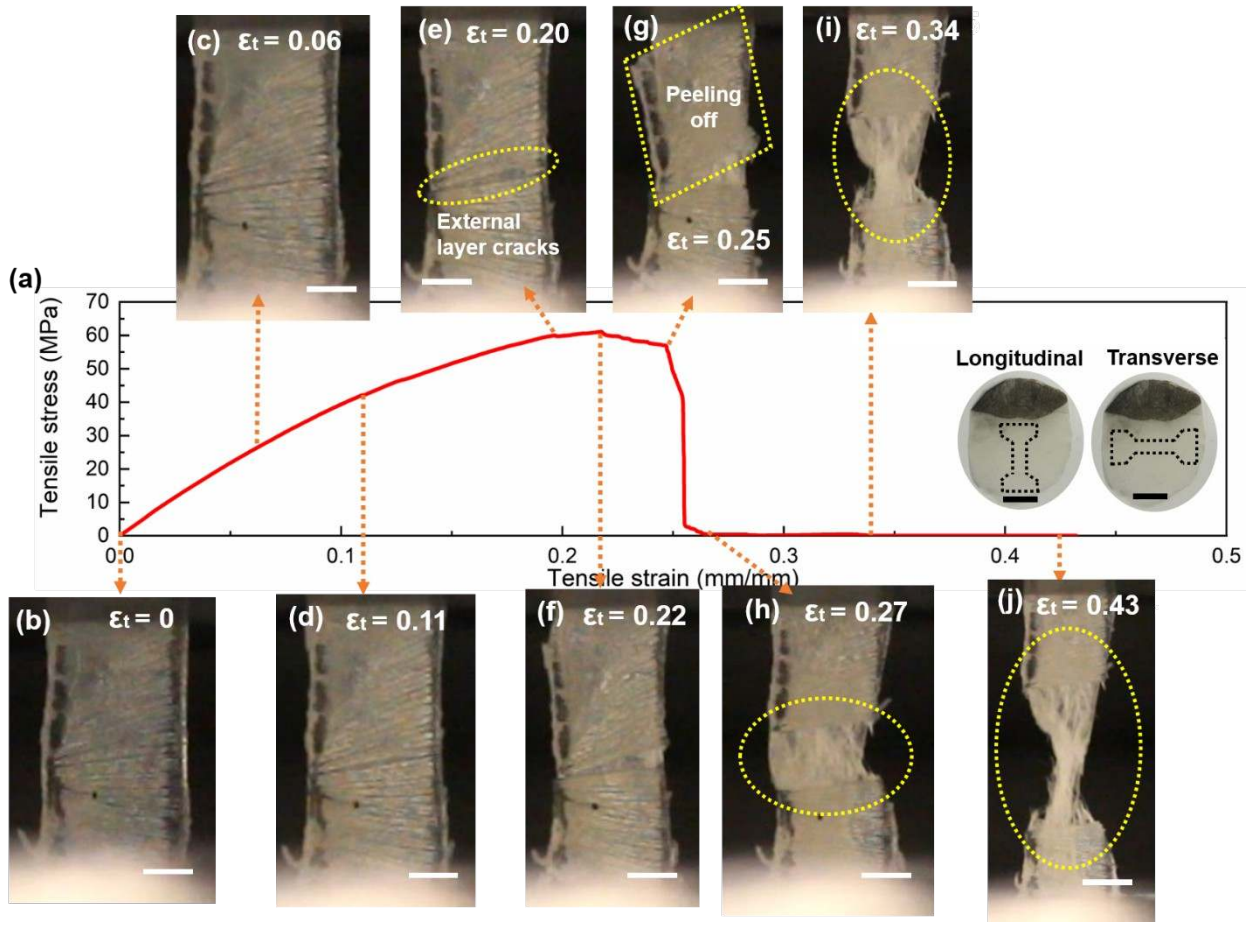

Figure 4 | A representative uniaxial tensile stress-strain curve of carp scales with images at different tissue strains (ε_t). (**a**) Tensile stress-strain curve of a dog-bone shaped specimen cut along the transverse direction. The orientations of tensile testing specimens are indicated in the inset. (**b-d**) Tensile specimen is being stretched in the linear region. (**e**) The external layer starts to crack. (**f**) The crack grows, and the external layer starts to separate from the inner collagenous layer. (**g**) The mineral layer peels off the scale. (**h-j**) The tissue has already failed. Some collagen fibrils are still being stretched although the load has dropped to almost zero. Scale bars for insets in (a), 5 mm. Scale bars for (b-j), 1 mm.

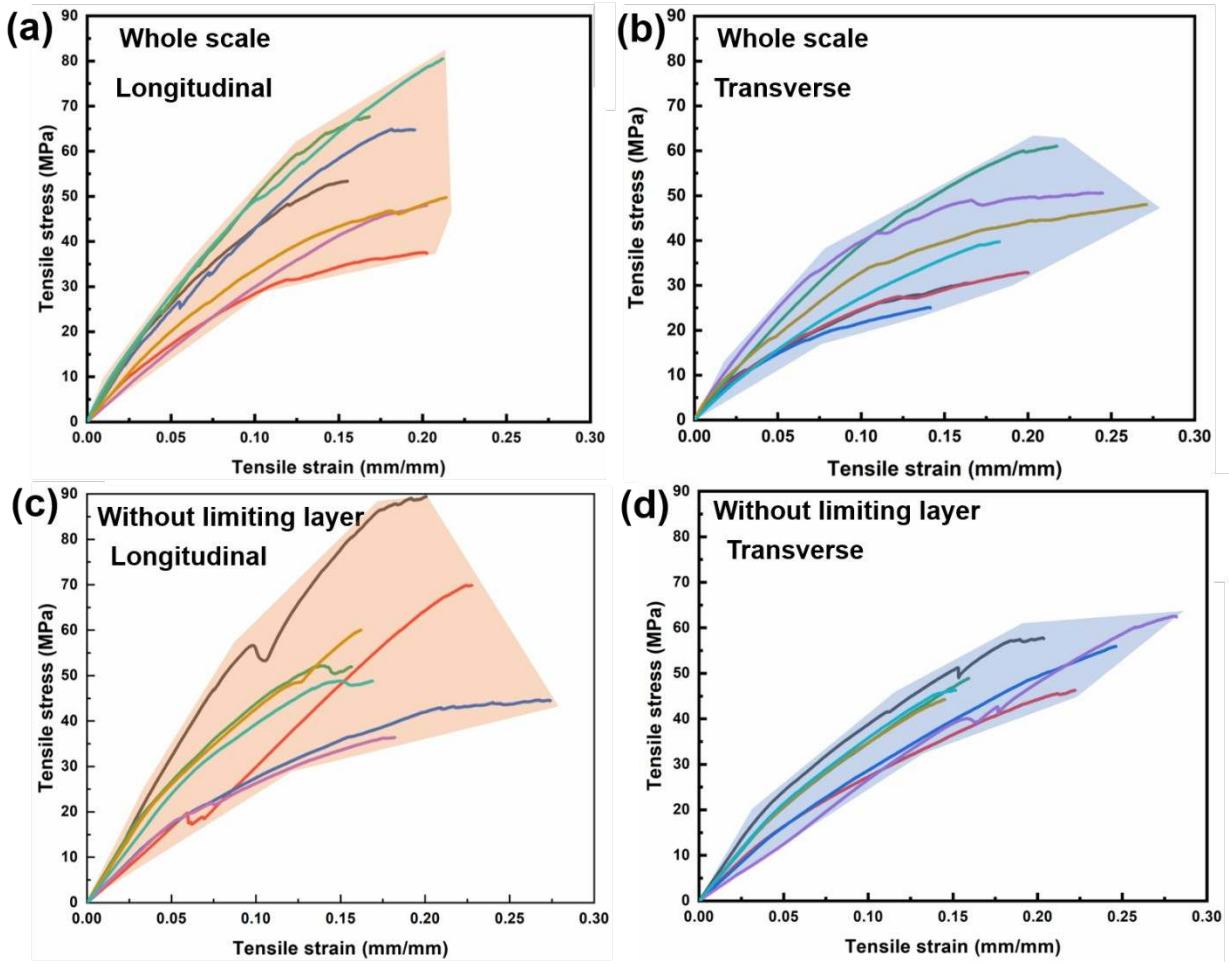

Figure 5 | Tensile behavior of carp scales in different orientations and conditions. (**a**,**b**) Uniaxial engineering stress-strain curves of whole scales along the longitudinal and transverse directions, respectively. (**c**,**d**) Uniaxial stress-strain curves, respectively along the longitudinal and transverse directions, of samples without the limiting layer (which was mechanically removed).

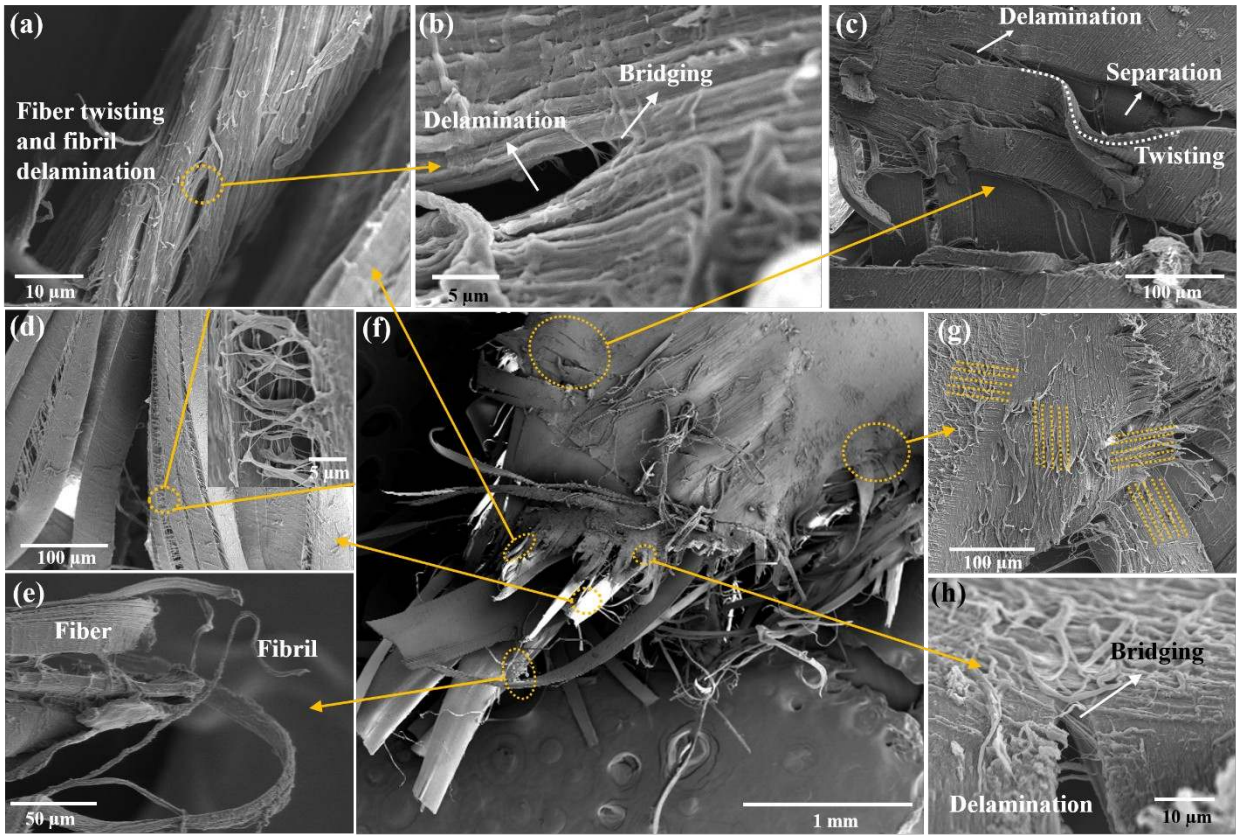

Figure 6 | Fracture surfaces after tensile failure of the carp scale. (**a**-**h**) SEM images of a fractured tensile specimen in different regions reveals multiple failure mechanisms. (**a**) The collagen fibers become twisted and start to delaminate. Scale bar, 10 μm. (**b**) A close-up view of the delaminated fibrils shows crack bridging near the tip of the delamination. Scale bar, 5 μm. (**c**) Delamination occurring in the same lamella with layer separation between two adjacent lamellae; the collagen fiber in the top lamella becomes twisted after separation. Scale bar, 100 μm. (**d**) Delamination and fibrillar bridging between collagen fibers. Scale bar, 100 μm. The scale bar for inset, 50 μm. (**e**) Fractured collagen fibers and fibrils. Scale bar, 50 μm. (**f**) An overall view of a fractured tensile specimen. Scale bar, 1 mm. (**g**) The four sets of dotted lines indicate the orientations of four neighboring lamellae. The irregular fibrous surface reveals the ductile separation between these layers as the tissue was being deformed. Scale bar, 100 μm. (**h**) Fibrillar delamination and crack bridging in a single collagen lamella. Scale bar, 10 μm..

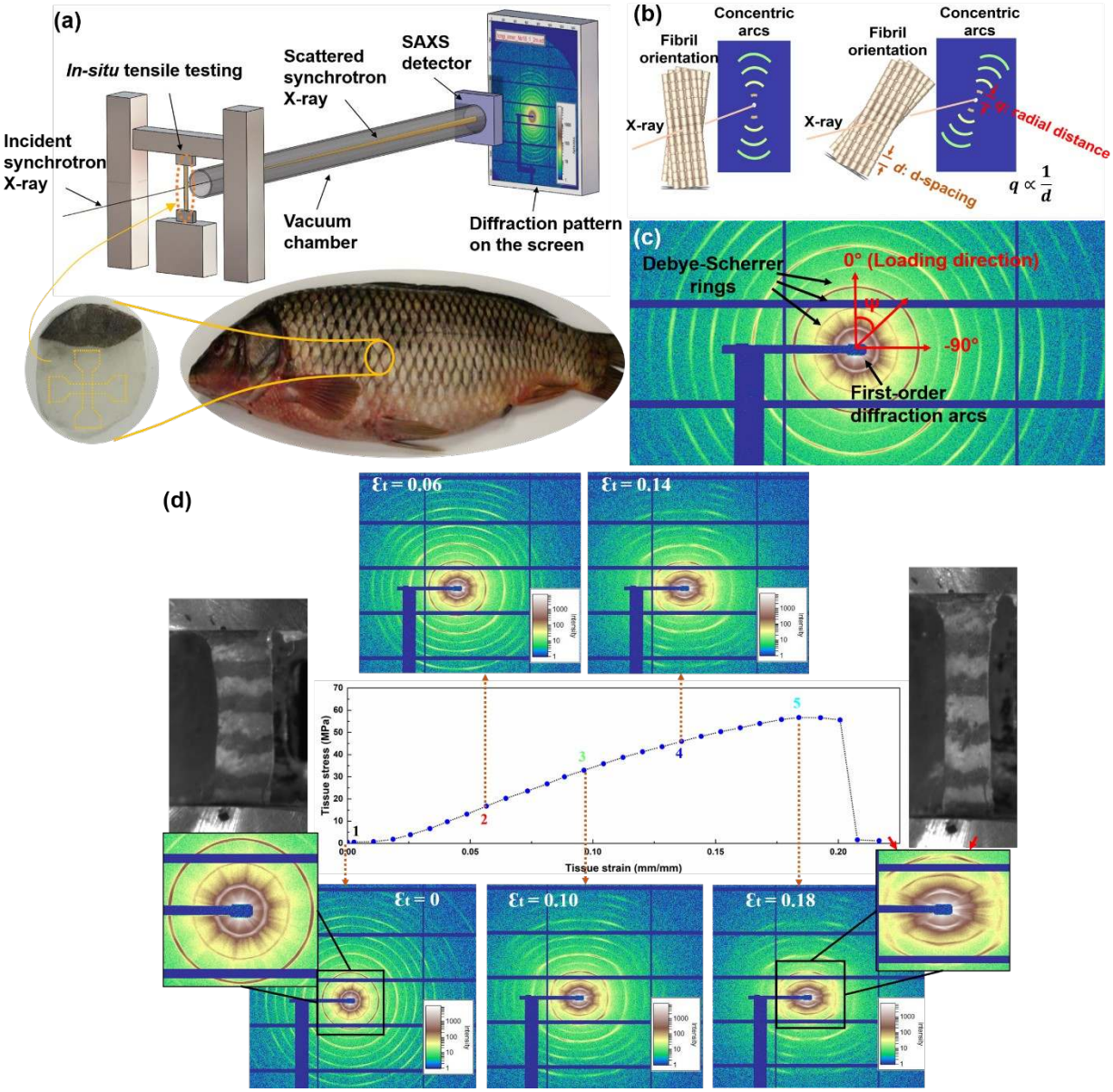

Figure 7 | *In situ* small-angle x-ray scattering (SAXS) patterns of carp scales taken in real time during a uniaxial tensile test. (**a**) Experimental set-up. Tensile specimens are extracted from the overlapped region of the scales along both longitudinal and transverse directions and the mineral layer is removed mechanically. The prepared specimen is exposed to the synchrotron x-rays in the beamline at the Advanced Light Source during *in situ* uniaxial tensile tests, with the scattering patterns recorded as a function of the tissue strain in real time. (**b**) Schematic showing the reciprocal relationship between the radius of the first-order arc (q) and the d-spacing of the collagen fibrils, based on the Bragg's law. (**c**) Pattern of a fully relaxed longitudinal sample shows several sets of concentric arcs, each of them caused by the diffraction of collagen fibrils well aligned in certain directions, which are the lamellar orientations in the fish scale. The loading direction is defined as the azimuthal angle (Ψ) equal to 0°. (**d**) *In situ* SAXS patterns at five different tissue strains (ε_t = 0, 0.06, 0.10, 0.14, and 0.18) in the tensile test of a longitudinal

sample. The insets in the patterns of the fully relaxed state ($\varepsilon_t = 0$) and highest stress state ($\varepsilon_t = 0.18$) are the close-up views of first several Debye-Scherrer rings with the real-time images of the tissue. The diffraction pattern changes from a round circle with six equal sectors to a hexagon-like shape, revealing the inhomogeneous deformation of the fibrils in different orientations.

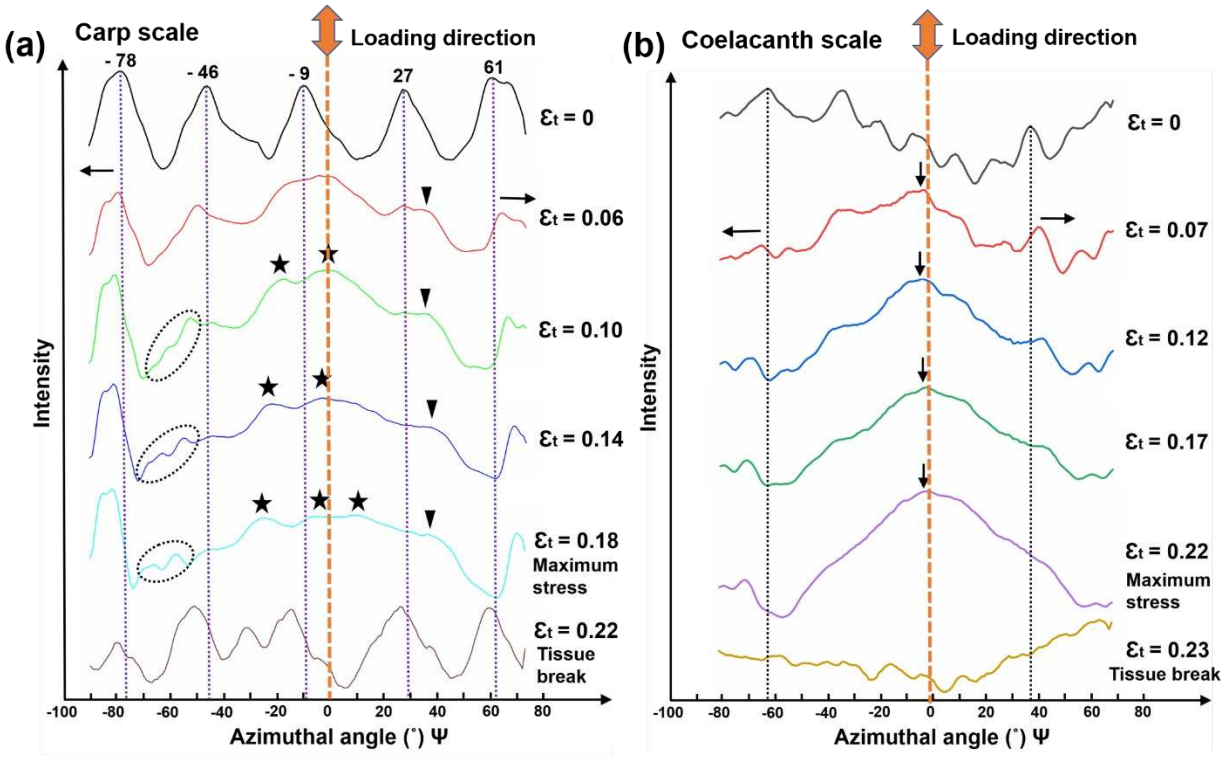

Figure 8 | Quantification of the rotation of collagenous lamellae for the carp scale under tensile loading in comparison with that for the coelacanth scale. (**a**) Curves of the integrated diffraction intensity *vs*. azimuthal angle (Ψ) for the carp scale at different deformation states (ε_t = 0, 0.06, 0.10, 0.14, 0.18 and 0.22). (**b**) Corresponding curves of integrated diffraction intensity *vs*. azimuthal angle (Ψ) for the coelacanth scale at different deformation states (ε_t = 0, 0.07, 0.12, 0.17, 0.22 and 0.13).

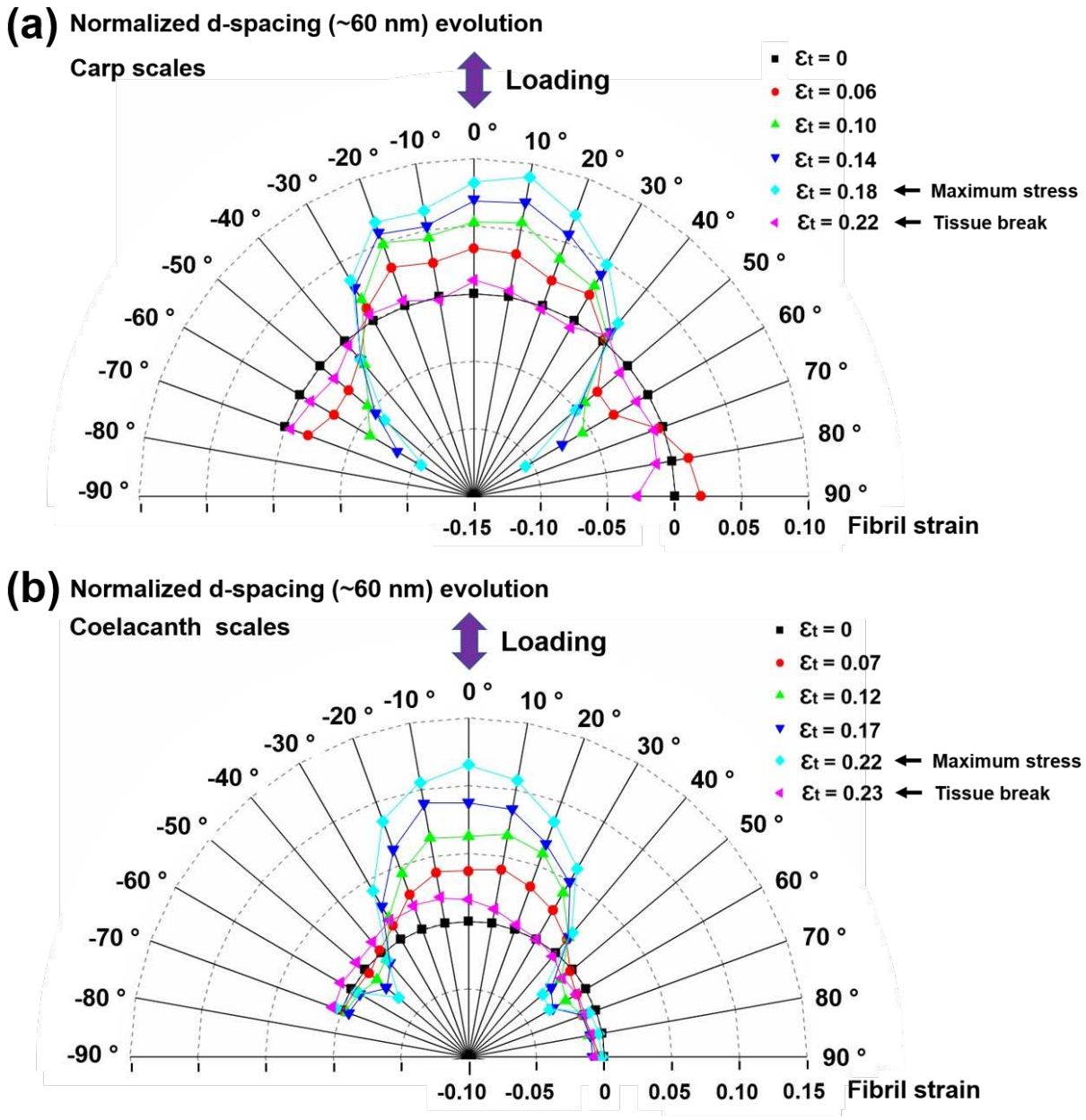

Figure 9 | Quantification of the deformation of collagen fibrils under tensile load in the carp scale as compared to the coelacanth scale. (**a**) Plots of fibril strain as a function of the azimuthal angle Ψ for the carp scale at different tissue strains (ε_t = 0, 0.06, 0.10, 0.14, 0.18 and 0.22). (**b**) Corresponding plots of fibril strain as a function of the azimuthal angle for the coelacanth scale at different tissue strains (ε_t = 0, 0.07, 0.12, 0.17, 0.22 and 0.23). For each scale, the fibril strain is calculated from the change in *d*-spacing along the collagen fibril during the tensile test and divided by the *d*-spacing of the fibrils in their original (unloaded) state.

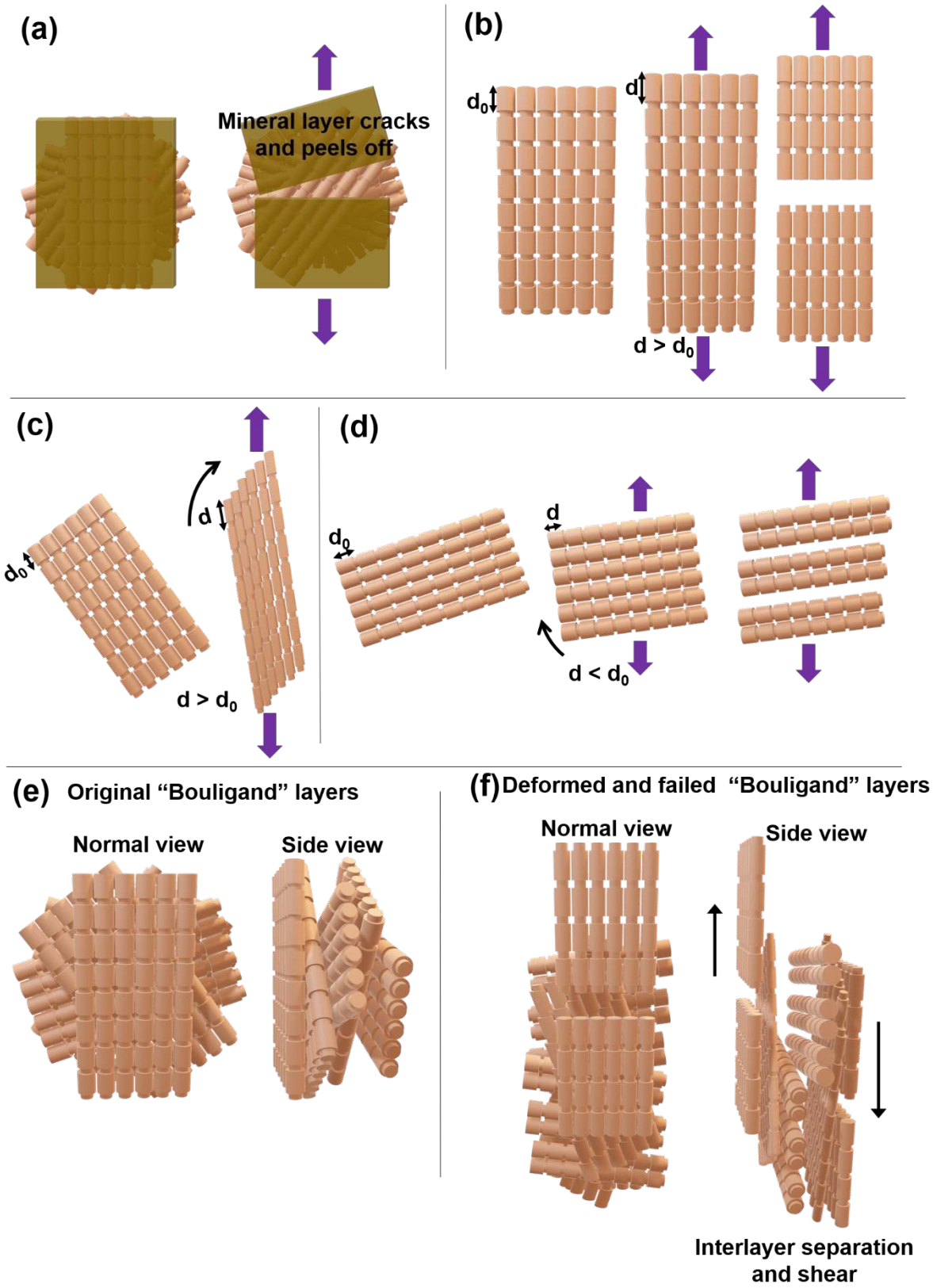
(a)
Mineral layer cracks and peels off
(b)
d_0
d
$d > d_0$
(c)
d_0
d
$d > d_0$
(d)
d_0
d
$d < d_0$
(e) Original "Bouligand" layers
Normal view
Side view
(f) Deformed and failed "Bouligand" layers
Normal view
Side view
Interlayer separation and shear

Figure 10 | Schematic rendition showing the mechanisms for the adaptive deformation of the carp scale under tensile loading. The purple arrows indicate the loading direction. (**a**) The mineral layer cracks and separates from collagenous base. (**b**) The lamellae along the tensile direction are stretched ($d > d_0$) and finally break as loading increases. (**c**) Interfibrillar sliding causes the lamellae to rotate towards the loading direction (as the black arrow indicates) and the collagen fibrils are also stretched, with increased d-spacing ($d > d_0$). (**d**) The lamellae initially oriented far from tensile axis are compressed ($d < d_0$) and rotate away (as the black arrow indicates). With further increase in loading, the lamellae fail by interfibrillar delamination. (**e**) The original collagenous lamellae form a highly ordered Bouligand-type structure with a rotation angle of 36°. (**f**) The overall deformed collagenous lamellae with applied tensile load. Combining all the adaptive mechanisms in (**b**-**d**) and the separation and shear between lamellae, the fibrous base confers the scale with significant deformability to adapt to the applied load.

Table 1

Uniaxial tensile test results in both longitudinal and transverse directions for the whole carp scale and for the collagen layer only.

Carp scale	**Whole scale**		**Collagen layer**	
	Longitudinal	**Transverse**	**Longitudinal**	**Transverse**
Young's Modulus (MPa)	521.5 ± 125	463.5 ± 92.3	526.0 ± 126.1	406.4 ± 95.5
Ultimate tensile stress (MPa)	57.4 ± 14.5	41.4 ± 12.8	57.3 ± 17.8	51.7 ± 7.00
Ultimate tensile strain (mm/mm)	0.193 ± 0.023	0.206 ± 0.047	0.196 ± 0.043	0.201 ± 0.005
Energy dissipation (MJ/ m^3)	6.79 ± 1.75	5.83 ± 2.90	6.8 ± 2.31	6.22 ± 2.23

SUPPLEMENTARY INFORMATION

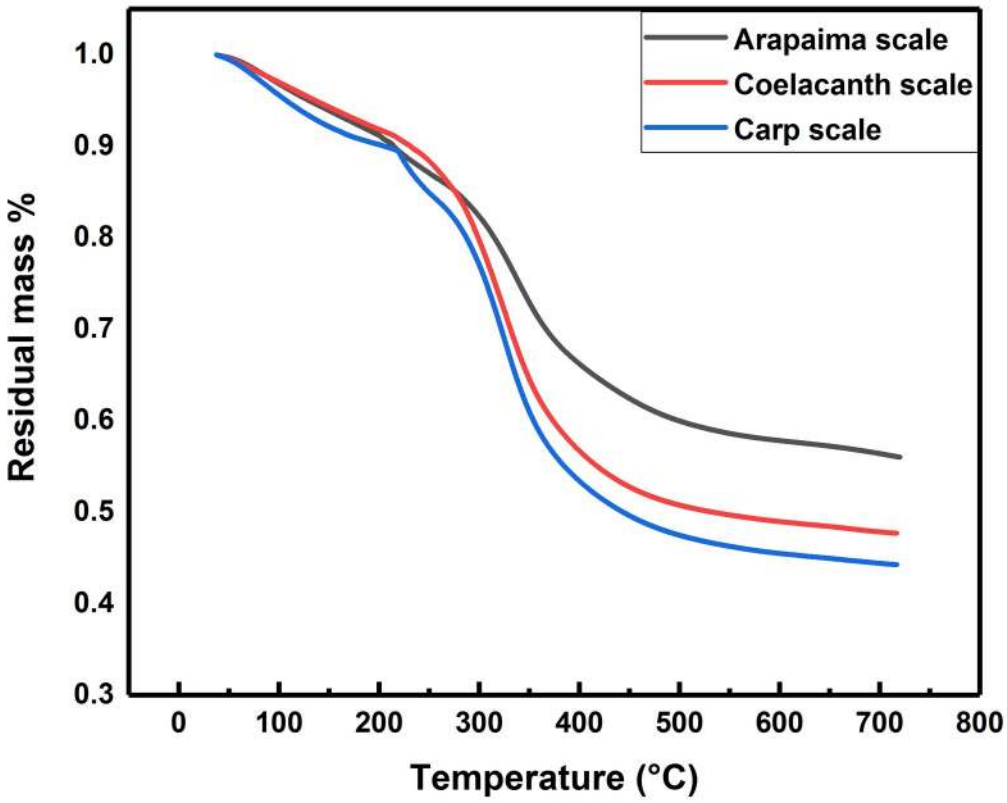

Figure S1 | Thermogravimetric analysis (TGA) of elasmoid scales from the carp, coelacanth, and arapaima fish. Between 250° and 400°C, there is a significant decrease in weight due to the oxidation of organic components, leaving only the mineral residue. The carp scale has lowest residual mass after the temperature is increased to 700°C, indicating it has the lowest mineral content compared with the coelacanth and arapaima scales.

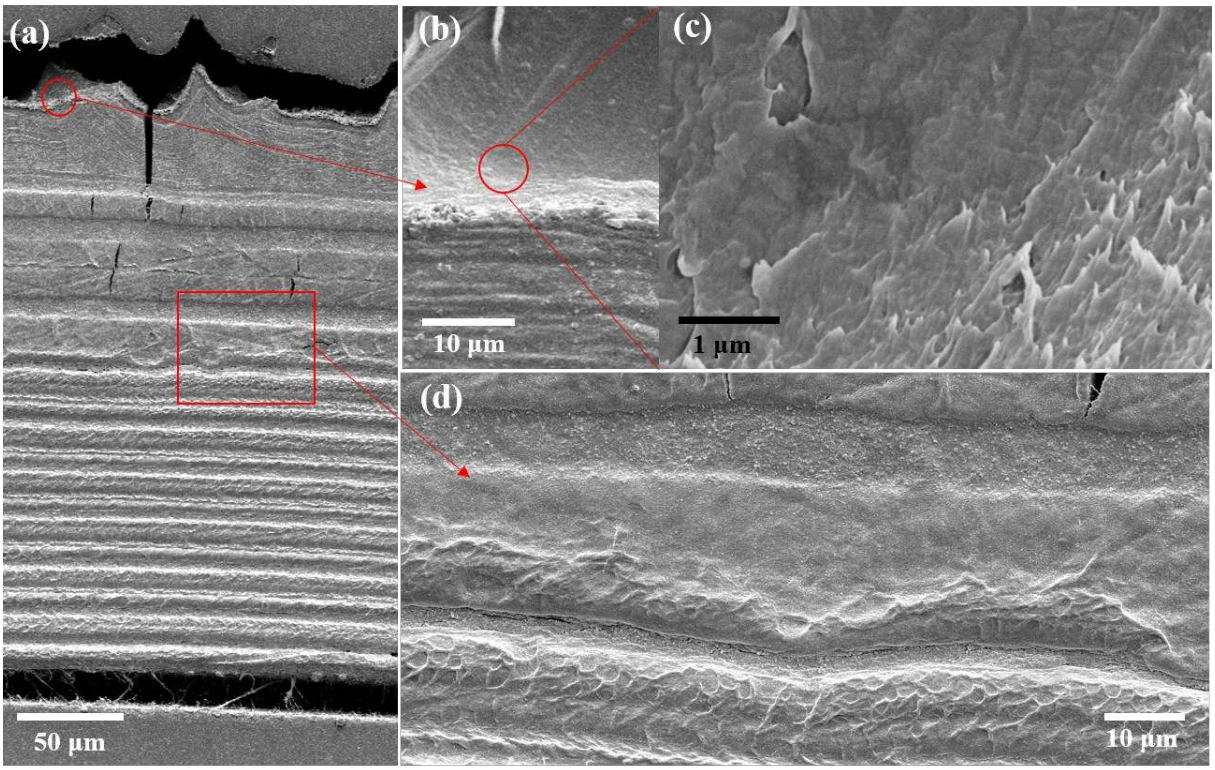

Figure S2 | The multilayered structure in the carp scale. (**a**) SEM images of a polished cross-section. (**b**,**c**) Close-up view of the limiting layer reveals the fibrous structure is exposed on the surface. (**e**) Close-up view of a polished cross-section of the elasmodine layer shows the outer (upper) region; this layer shows a less fibrous structure compared with the inner (bottom) region, indicating that the latter region is less mineralized.

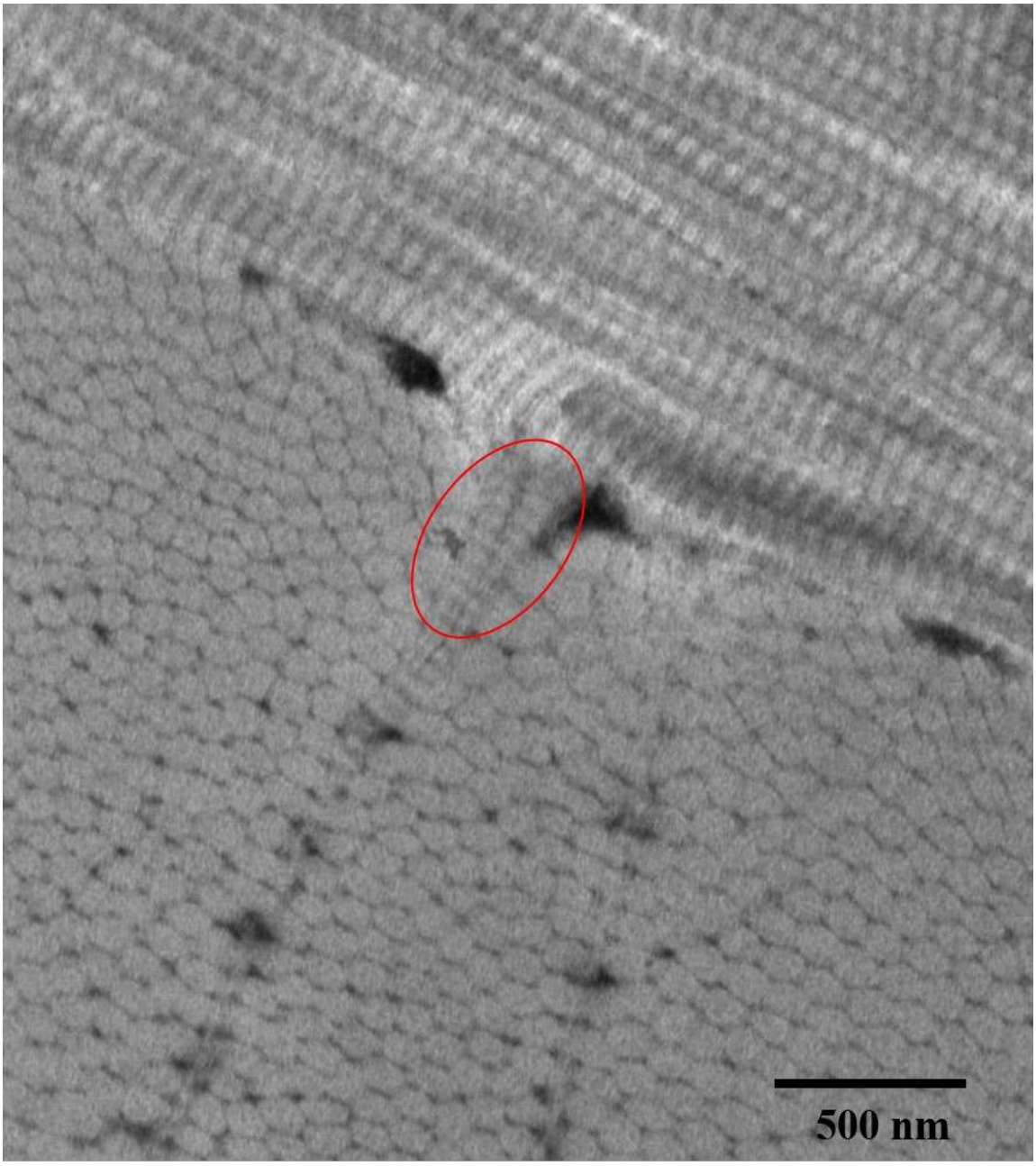

Figure S3 | TEM image of a cross-section of the carp scale. It shows that the secondary collagenous network through the thickness direction is not composed of a single collagen fibril, as marked with the red circle.

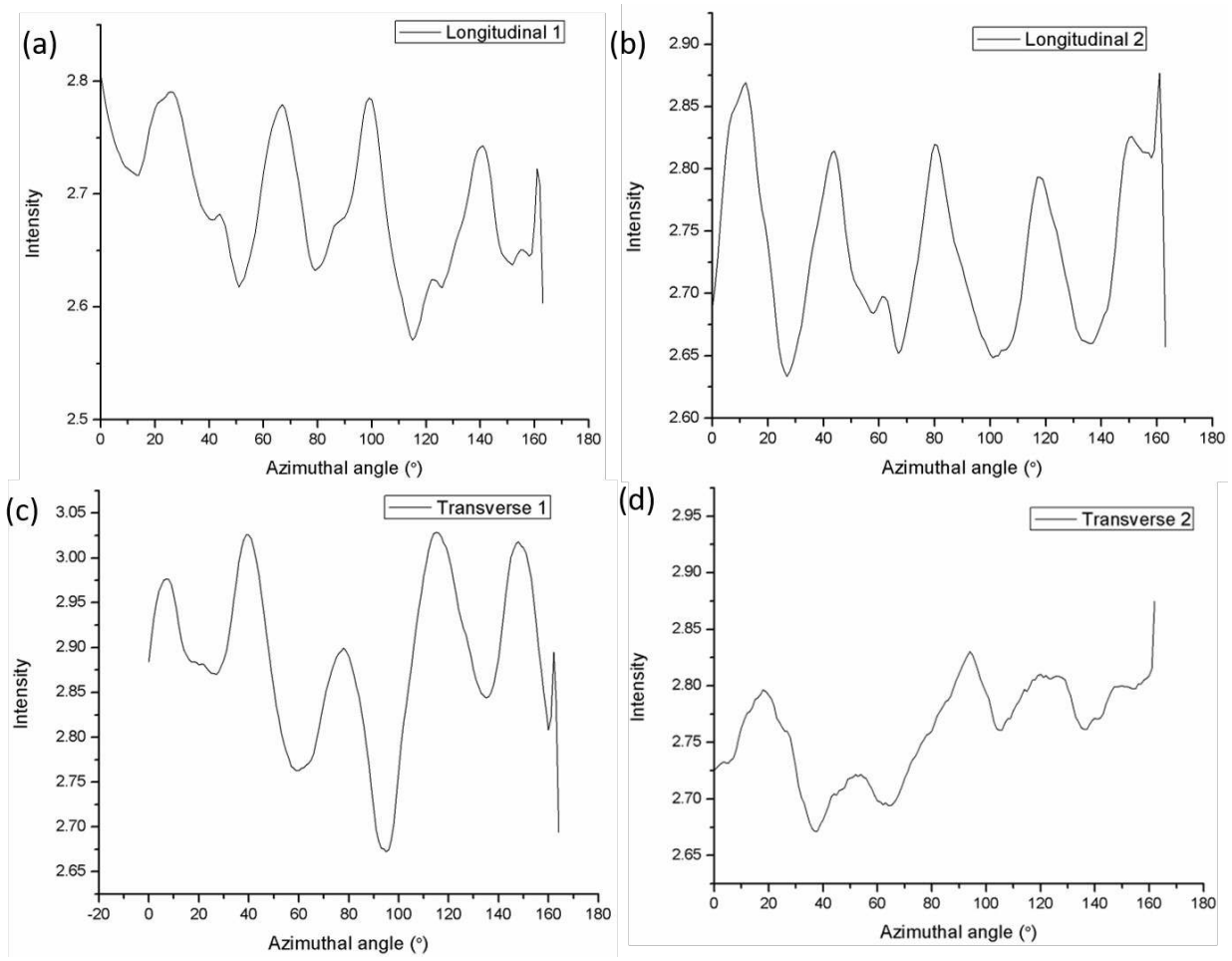

Figure S4 | The twist angle of single-twisted Bouligand structure. (**a-d**) Curves of integrated diffraction intensity *vs*. azimuthal angle (Ψ) for 4 scale specimens at full rest state. The space between diffraction peaks is consistently ~36˚.

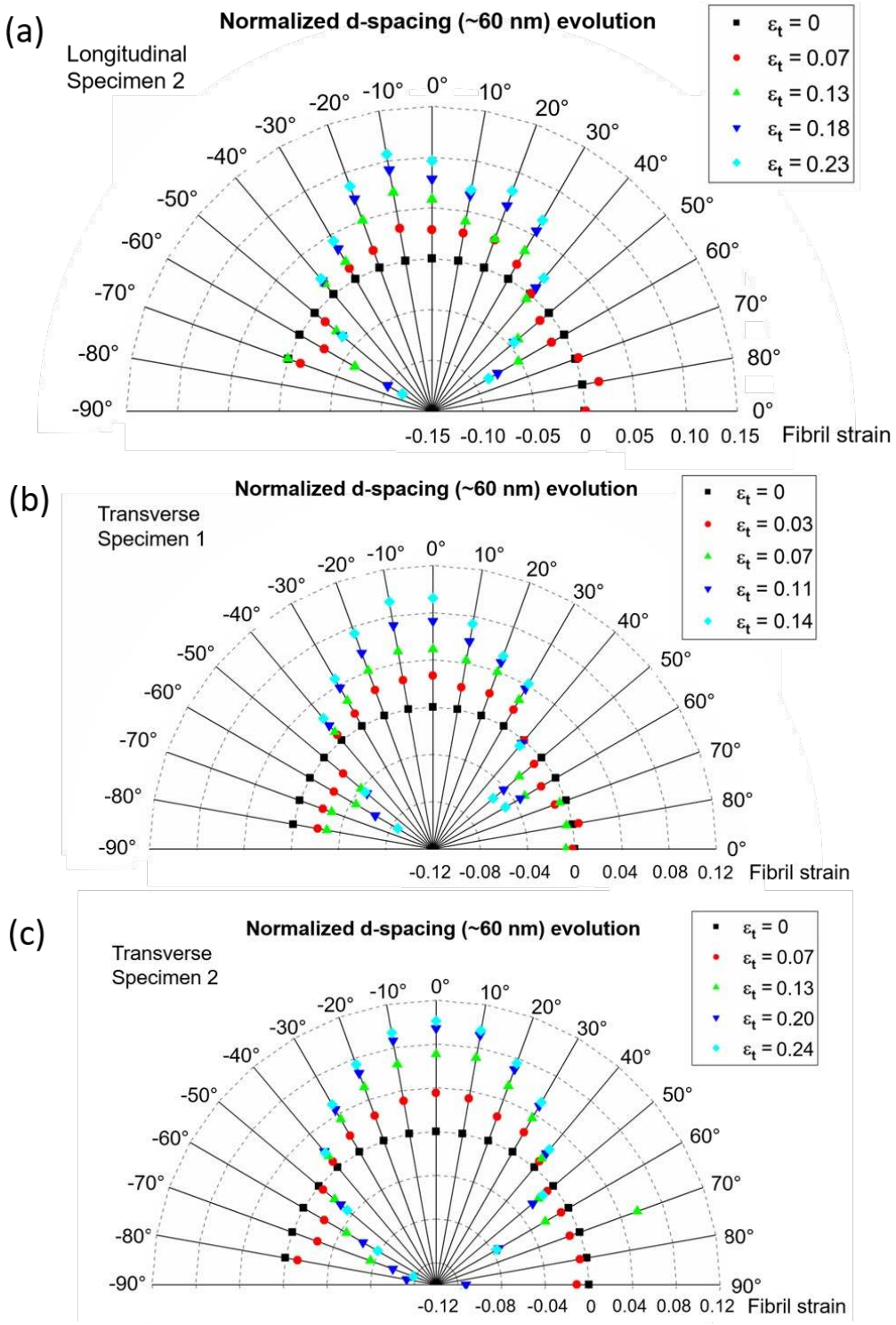

Figure S5 | The deformation of collagen fibrils under tensile load for three additional specimens. (**a**) Plots of fibril strain as a function of the azimuthal angle Ψ for a longitudinal specimen at different tissue strains (ε_t = 0, 0.07, 0.13, 0.18, 0.23). (**b,c**) The same plot for two transverse specimens at (**b**) ε_t = 0, 0.03, 0.07, 0.11, 0.14 and (**c**) ε_t = 0, 0.03, 0.07, 0.11, 0.14.

Reciprocal Relationship Between *q* and *d*

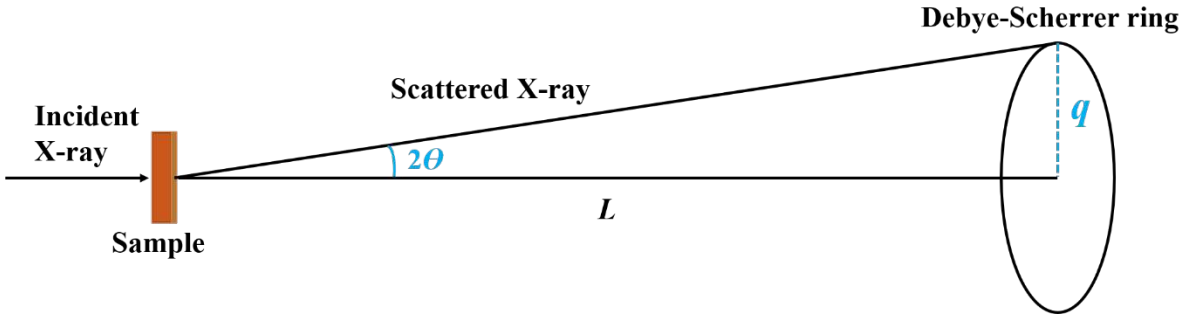

Figure S6 | Schematic diagram showing the x-ray diffraction set-up using Debye-Scherrer method. ***q*** is the radius of the diffraction pattern; ***L*** is the distance between the sample and the detector.

$$\tan 2\theta = \frac{q}{L}$$

Since θ is very small, $\sin\theta \sim \tan\theta \sim \theta$.

$$\tan 2\theta = 2\theta = \frac{q}{L}$$

$$\theta = \frac{q}{2L}$$

Bragg's law: $2d\sin\theta = n\lambda$

$$\sin\theta = \frac{n\lambda}{2d}$$

$$\theta = \frac{n\lambda}{2d}$$

Therefore,

$$\frac{q}{2L} = \frac{n\lambda}{2d}$$

If we only consider about the first-order diffraction, n =1,then $d=\frac{\lambda L}{q}$.

During the deformation, the strain in each collagen fibril, $\boldsymbol{\varepsilon_f}$, is:

$$\varepsilon_f=\frac{d-d_0}{d_0}=\frac{d}{d_0}-1=\frac{\frac{\lambda L}{q}}{\frac{\lambda L}{q_0}}-1=\frac{q_0}{q}-1\ ,$$

where $\boldsymbol{d_0}$ is the d-spacing in undeformed collagen and $\boldsymbol{d}$ is the spacing after deformation, and $\boldsymbol{q_0}$ is the radius of diffraction ring in the unloaded specimen. This results shows that the fibril strain ε_f has a reciprocal relationship with the radius of the diffraction pattern, $\boldsymbol{q}$.